

Redox-regulation of photorespiration through mitochondrial thioredoxin o1

Ole Reinholdt, Saskia Schwab, Youjun Zhang, Jean-Philippe Reichheld, Alisdair Fernie, Martin Hagemann, Stefan Timm

▶ **To cite this version:**

Ole Reinholdt, Saskia Schwab, Youjun Zhang, Jean-Philippe Reichheld, Alisdair Fernie, et al.. Redox-regulation of photorespiration through mitochondrial thioredoxin o1. Plant Physiology, 2019, 181 (2), pp.442-457. 10.1104/pp.19.00559 . hal-02290017

HAL Id: hal-02290017

https://univ-perp.hal.science/hal-02290017

Submitted on 27 Jan 2020

HAL is a multi-disciplinary open access archive for the deposit and dissemination of scientific research documents, whether they are published or not. The documents may come from teaching and research institutions in France or abroad, or from public or private research centers.

L'archive ouverte pluridisciplinaire **HAL**, est destinée au dépôt et à la diffusion de documents scientifiques de niveau recherche, publiés ou non, émanant des établissements d'enseignement et de recherche français ou étrangers, des laboratoires publics ou privés.

Redox-regulation of photorespiration through mitochondrial thioredoxin o1

Ole Reinholdt[1§], Saskia Schwab[1], Youjun Zhang[2,3], Jean-Philippe Reichheld[4,5], Alisdair R. Fernie[2,3], Martin Hagemann[1], and Stefan Timm[1*]

[1]University of Rostock, Plant Physiology Department, Albert-Einstein-Straße 3, D-18059 Rostock, Germany

[2]Max Planck Institute of Molecular Plant Physiology, Am Mühlenberg 1, D-14476 Golm, Germany

[3]Center of Plant System Biology and Biotechnology, 4000 Plovdiv, Bulgaria

[4]Laboratoire Génome et Développement des Plantes, CNRS, F-66860 Perpignan, France;

[5]Laboratoire Génome et Développement des Plantes, Université Perpignan Via Domitia, F-66860 Perpignan, France

***Correspondence to** stefan.timm@uni-rostock.de

+49 381 498 6115 (fon) -6112 (fax)

§Footnotes

Present address of O.R.: Miltenyi Biotec GmbH, Robert-Koch-Straße 1, 17166 Teterow, Germany.

Abstract

Photorespiration sustains photosynthesis in the presence of oxygen due to rapid metabolization of 2-phosphoglycolate (2-PG), the major side-product of the oxygenase activity of Rubisco. This metabolic intermediate has additionally been shown to directly impede carbon assimilation and allocation. Despite the fact that both, the biochemical reactions and the underlying genetics are well characterized, information concerning the regulatory mechanisms which adjust photorespiratory flux is rare. Here, we studied the impact that the mitochondrial localized thioredoxin o1 (TRXo1) has on photorespiratory metabolism. The characterization of a T-DNA insertional line (*trxo1*) revealed an increase in the stoichiometry of photorespiratory CO_2 release and impaired glycine-to-serine turnover after a shift from high-to-low CO_2, without changes in glycine decarboxylase (GDC) expression. These effects were distinctly pronounced in a double mutant, where the *TRXo1* mutation was combined with strongly reduced GDC T-protein expression. The double mutant (*TxGT*) showed reduced growth in air, but not in high CO_2, decreased photosynthesis and accumulated up to 54-fold more glycine alongside several redox-stress-related metabolites. Given that GDC proteins are potential targets for redox-regulation, we also examined the *in vitro* properties of recombinant GDC L-proteins (LPD) from plants and the cyanobacterium Synechocystis and observed a redox-dependent inhibition by either artificial reducing agents or TRXo1 itself. Collectively, our results demonstrate that TRXo1 potentially adjusts photorespiration via redox-regulation of GDC in response to environmental changes.

Introduction

Photorespiration is an essential process in all organisms performing oxygenic photosynthesis, because it is intrinsically linked to photosynthetic CO_2 fixation via Rubisco that catalyzes the carboxylation but also oxygenation reaction (Bauwe et al., 2012; Appel et al., 2013). During carboxylation, CO_2 is incorporated into the acceptor ribulose-1,5-bisphosphate (RuBP) leading to the formation of two 3-phosphoglycerate (3-PGA) molecules that enter the Calvin-Benson cycle (CBC). In the Rubisco oxygenase reaction RuBP can also accept O_2 yielding one 3PGA and one 2-phosphoglycolate (2-PG) molecule (Bowes et al., 1971). 2-PG is a non-CBC intermediate that is exclusively metabolized by the photorespiratory C2 cycle (Somerville and Ogren, 1979). In addition to the main function of photorespiration as organic carbon salvage pathway, efficient 2-PG degradation is essential for plant metabolism, because 2-PG acts as a potent inhibitor of many enzymes in the chloroplastidial stroma, such as triose-phosphate isomerase, phosphofructokinase and sedoheptulose-1,7-bisphosphate phosphatase (Anderson, 1971; Kelly

and Latzkow, 1976; Flügel et al., 2017; Levey et al., 2019; Li et al., 2019). Hence, 2-PG accumulation significantly reduces the efficiency of CO_2 assimilation through impairment of the CBC and starch biosynthesis.

Following the early discovery of the light-induced photorespiratory gas-exchange (Zelitch, 1964; Tolbert, 1971; Ogren and Bowes, 1976), a broad range of photorespiratory mutants of the C3 plants Arabidopsis, barley, pea, and tobacco, were generated to facilitate the molecular analysis of this important process. These mutants showed the characteristic photorespiratory phenotype, i.e. they could not grow at ambient air conditions but could be rescued in the presence of enhanced CO_2 supplementation (e.g. summarized in: Blackwell et al., 1988; Leegood et al., 1995; Somerville, 2001; Timm and Bauwe, 2013). More recently, photorespiratory mutants of organisms performing a carbon concentrating mechanism such as cyanobacteria, red and green algae (Suzuki et al., 1989; Nakamura et al., 2005; Eisenhut et al., 2008; Rademacher et al., 2016) as well as C4 plant species (Zelitch et al., 2009; Levey et al., 2019) were obtained, which also showed the photorespiratory phenotype, supporting the view of photorespiration as essential partner of photosynthesis in oxygen-rich atmospheres. The detailed physiological and molecular characterization of all these mutants has generated a comprehensive picture of photorespiration, including the biochemical pathway, the underlying genetics and how photorespiration is embedded in the network of primary metabolism and interacts with many other pathways within the entire cellular context (e.g. reviewed in: Wingler et al., 2000; Reumann and Weber, 2006; Foyer et al., 2009; Bauwe et al., 2010; 2012; Fernie et al., 2013; Hodges et al., 2016; Obata et al., 2016; Timm et al., 2016).

In contrast to our broad knowledge on function of photorespiration, less progress has been made with regards to potential regulatory mechanisms within the photorespiratory cycle. Existing data indicate that the mitochondrial glycine-to-serine interconversion, catalyzed through glycine-decarboxylase (GDC) in conjunction with serine-hydroxymethyltransferase (SHMT1), potentially represent target sites for the regulation of photorespiration. The importance of the GDC and SHMT reactions are based on three facts. First, during glycine-to-serine conversion, CO_2 and ammonia are liberated. Hence, this step of photorespiration emerged as the prime target for genetic engineering approaches to increase crop productivity (Peterhänsel et al., 2013; Betti et al., 2016; Walker et al., 2016; South et al., 2018). Secondly, GDC activity was found to be a key component in the control of photosynthesis and plant growth (Timm et al., 2012; 2015; 2016; Simkin et al., 2017; López-Calcagno et al., 2018). Thirdly, the GDC reaction cycle requires four cooperating proteins GDC-P, GDC-T, GDC-H and GDC-L, where the latter is also involved in the

reaction cycle of other enzymatic complexes, which indicates that this biochemical activity needs proper regulation (Douce et al., 2001; Timm et al., 2015).

It has been already shown that, in addition to light-induced transcriptional and translational activation of GDC (Walker and Oliver, 1986; Vauclare et al., 1996; Timm et al., 2013), the GDC activity in plant mitochondria appears to be sensitive to redox changes. Especially, the NADH and NAD^+ levels are of importance, thereby an increased NADH/NAD^+ ratio strongly impedes glycine-to-serine turnover (Bourguignon et al., 1988). Isolated GDC could be also competitively inhibited by serine (K_i ~ 4 mM) (Oliver and Sarojini, 1987). Finally, GDC activity can be also modulated via post-translational modification. For example, Palmieri et al (2010) showed regulation of GDC activity by *S*-nitrosylation and *S*-glutathionylation of GDC-H and GDC-P, respectively. Moreover, Hodges et al. (2013) reported phosphorylation of several GDC proteins and proposed that those modifications might contribute to activity regulation. Proteomic analyses provided evidence that all four GDC proteins contain conserved cysteine residues and therefore might undergo redox-regulation *in vivo* (Balmer et al., 2004; Keech et al., 2017; Pérez-Pérez et al., 2017). Indeed, it was demonstrated that recombinant cyanobacterial GDC P-protein could be activated under reducing conditions (Hasse et al., 2013).

The above-mentioned results make it likely that the glycine-to-serine interconversion is modulated via redox-regulation at multiple points. Hence, we investigated whether a mitochondrial thioredoxin (TRXo1) is involved in the potential redox regulation of photorespiratory reactions in this compartment. To this end, we compared the photosynthetic gas-exchange and the metabolic acclimation toward altered CO_2 partial pressure and light conditions of the T-DNA insertional line *trxo1* (*trxo1-1*; Daloso et al., 2015) and a newly generated double mutant (*TxGT*), which is defective in *TRXo1* expression and strongly reduced in the GDC T-protein (*gldt1-1*; Timm et al., 2018). Moreover, we performed *in vitro* LPD activity measurements using isolated mitochondria or recombinant proteins to provide direct experimental evidence for redox-regulation of GDC. Collectively, our results provide evidence that TRXo1 is involved in the regulation of mitochondrial photorespiration and thus contributes to the adaptation of the photorespiratory flux towards changes in the environmental conditions that affect the subcellular redox-state.

Results

Deletion of *TRXo1* causes an increase in the stoichiometry of photorespiratory CO_2 release

In general, mutants defective in photorespiration or associated processes exhibit a distinct negative impact on the photosynthetic gas exchange (e.g. Dellero et al., 2015; Eisenhut et al., 2013a; Pick et al., 2013; Timm et al., 2012). Apart from constraints within the core cycle, deletion of genes that encode for proteins of accessory functions were characterized by an increase in the stoichiometry of photorespiratory CO_2 release, particularly under conditions that require photorespiration to operate at high efficiencies (Cousins et al., 2011; Timm et al., 2011). To test whether *TRXo1* mutation impacts photorespiratory metabolism, the T-DNA insertional line *trxo1* (*trxo1-1*; Daloso et al., 2015) and the wild type were subjected to varying oxygen concentrations (3, 21, 40, and 50% O_2) during gas exchange measurements. As shown in Fig. 1A, *trxo1* showed no alteration in the net CO_2 assimilation rate (A) at low or normal photorespiratory flux (3 and 21% O_2), which is in agreement with unaltered growth in normal air (Daloso et al., 2015), but significant decreased photosynthesis at enhanced O_2 concentrations (40 and 50%) that stimulate a higher flux through photorespiration. Hence, O_2 inhibition of A (Fig. 1B) was significantly higher in *trxo1* (47.7 ± 4.0%) compared to the wild type (38.3 ± 4.1%). In accordance with the decrease in A, the CO_2 compensation point (Γ) is unchanged at 3 and 21% O_2 but significantly higher in *trxo1* at 40 and 50% O_2 (Fig. 1C). These changes increase the slope (γ) from the estimated Γ-versus-oxygen response lines to about 20% (Fig. 1D), indicating a higher fraction of CO_2 released from photorespiration.

Metabolic effects of *TRXo1* deficiency on glycine turnover and cellular redox components

To further substantiate whether mitochondrial localized TRXo1 (Daloso et al., 2015) contributes to mitochondrial photorespiration we next performed metabolomics during CO_2 transition using liquid chromatography coupled to tandem mass spectrometry (LC-MS/MS). Rationally, CO_2 concentrations were varied to distinguish between states with suppressed photorespiration (high CO_2, HC, 1500 ppm) and two stages with active photorespiration that are 1 and 9 h after transfer of the plants into normal air (390 ppm). For comparison, we included the GDC T-protein knockdown mutant *gldt1*, characterized by a ~70% reduction in total GDC activity (*gldt1-1*; Timm et al., 2018). In agreement with previous studies (Timm et al., 2012; Eisenhut et al., 2016), the glycine content of wild type increased (~3.8 fold) 9 h after the transfer into normal air (Fig. 2)

(Timm et al., 2012; Eisenhut et al., 2016). However, a distinct, intermitted glycine accumulation (~38 fold) was visible after 1 h in normal air. This accumulation kinetics was most pronounced but not restricted to glycine, since other photorespiratory intermediates such as glyxoxylate, 3-hydroxypyruvate (3HP), glycerate, and 3-PGA followed a similar trend (Fig. 2). Interestingly, the redox-related compounds glutathione (GSH), cysteine and cystine also followed the pattern of the photorespiratory intermediates. Serine, as the product of GDC/SHMT reactions, behaves almost inverse to the changes observed in glycine. The wild type shows a transient drop in serine after 1 h in normal air but its absolute amount returned to HC levels after 9 h in normal air (Fig. 2). Compared to wild type, the transient glycine accumulation in *trxo1* is much lesser pronounced (~ 4.2 fold), but its content is considerably higher (~43 fold) after 9 h in normal air (Fig. 2). The missing intermitted increase was also observed in the other photorespiratory intermediates, which were all lower after 1 h in normal air or invariant (glyoxylate, 3HP and glycerate) compared to the wild type after 9 h in normal air. Only 3-PGA, the primary carboxylation product of Rubisco, was significantly decreased in *trxo1* after 9 h in normal air (Fig. 2). No intermitted accumulation was also seen in the three redox components after 1 h whilst higher levels of GSH and cysteine were observed after 9 h in normal air in *trxo1*. As expected, reduction of GDC activity to ~30% impairs glycine-to-serine interconversion in *gldt1* and thus causes a nearly linear increase in glycine up to 71-fold after 9 h LC compared to HC, a trend that was also reflected in GSH, cysteine and cystine levels. Concerning the other photorespiratory intermediates, an increase in the upstream intermediate glyoxylate after 9 h in normal air was found. The downstream metabolites 3HP and glycerate were significantly decreased only after 1 h and invariant after 9 h in normal air. Only 3-PGA was lower in *gldt1* in these two time points (Fig. 2). Other than the wild type, *trxo1* and *gldt1* showed a continuous decrease in the GDC/SHMT reaction product serine after the shift into normal air. Unsurprisingly, these changes sum up to a gradually increasing glycine-to-serine ratio in both mutants, whereas the increase in the wild type is only on a short-term (Fig. 2). From these results one can conclude that the most dominant effect is related to metabolites of GDC operation and redox regulation in both mutants.

Apart from changes in intermediates related to photorespiration and redox buffering, deletion of *TRXo1* also affected metabolite levels from the TCA-cycle. While several pathway intermediates (e.g. malate, citrate, fumarate and aconitate) show short-term accumulation followed by normalization or a steadily increase (succinate) in the wild type, they did not transiently increase and did not show major fluctuations during CO_2 transition in *trxo1* (Fig. 2; Supp. Table 1). A similar behavior was observed in *gldt1*, with the exception of an approximately 4-fold

accumulation of succinate. Finally, *gldt1* accumulates branched chain (valine, isoleucine and leucine) and aromatic (phenylalanine, tryptophan and tyrosine) amino acids upon the transfer into normal air as previously reported for other photorespiration mutants (Timm et al., 2012; Eisenhut et al., 2017; Orf et al., 2016). Again, *trxo1* behaved differently, since it showed only minor variations in the branched chain and aromatic amino acid contents after 9 h, but lacked the intermittent increases in the branched chain, but not aromatic amino acids, after 1 h in normal air as observed for wild type leaves (Fig. 2; Supp. Table S1).

Lack of *TRXo1* does not affect mRNA expression and protein abundance of photorespiratory genes/proteins

Given that the altered glycine-to-serine interconversion in *trxo1* could be due to an altered expression of the enzymes participating in photorespiration, we next analyzed mRNA and protein contents of enzymes involved in the mitochondrial steps of photorespiration. To this end, leaf-material of *trxo1* and the wild type was harvested at the end of the day (9 h illumination) in normal air and qRT-PCR and immuno-blotting experiments were carried out. As shown in Fig. 3, we never observed significant alterations in neither mRNA nor protein levels of all four GDC genes and the major photorespiratory SHMT1 isoform. Similarly, constant expression was also detected in all three genes that served as controls for photorespiratory enzymes not localized in the mitochondrion (Fig. 3), namely peroxisomal hydroxypyruvate reductase 1 (HPR1), peroxisomal malate dehydrogenase (pMDH) and chloroplastic 2-PG phosphatase (PGLP).

Deletion of *TRXo1* in the *gldt1* background intensifies the photorespiratory phenotype

Next we hypothesized that if TRXo1 affects GDC activity, phenotypic and physiological alterations would be exacerbated in mutants that exhibit combined defects in *TRXo1* and *GDC* expression under photorespiratory conditions. For this reason, *trxo1* was crossed with the *gldt1* knock-down mutant (5% residual *GDC-T* mRNA expression; Timm et al., 2018) to obtain the double mutant *TxGT* (for genotypic verification see Supp. Fig. S1). As shown in Fig. 4A, wild type and *trxo1* plants grew similarly (unchanged rosette diameter and leaf number) and were invariant from each other with regard to chlorophyll a fluorescence. In agreement with previous findings (Timm et al., 2018), *gldt1* showed reduced growth (reduction in the rosette diameter), yellowish leaves, and lowered F_v/F_m under photorespiratory conditions. Interestingly, the reduction of growth and PSII efficiency observed in the *gldt1* mutant was further enhanced in the *TxGT* line (Fig. 4A). The slower growth of *gldt1* and *TxGT* mutant lines also caused delayed onset of flowering for approximately one and three weeks, respectively. If plants were cultivated

in HC, suppressing photorespiration, growth of the *gldt1* and *TxGT* lines are fully restored to wild type levels as reflected by the unchanged rosette diameter and total leaf number, while *TxGT* still showed a significant decrease in F_v/F_m (Fig. 4B). Collectively, CO_2 dependent complementation of growth suggests that the stronger phenotypic alterations in *TxGT* are due to an additive, negative impact on photorespiration.

Mutation of *TRXo1* and *GDC-T* does not affect expression of photorespiratory proteins

To exclude that the intensified signs of the photorespiratory phenotype are due to altered expression of photorespiratory enzymes in the double mutant, we carried out immunoblot analysis from all mutants in comparison with the wild type in a CO_2 transfer experiment as done for metabolite profiling before. To this end, leaf material was harvested from 8 week old plants in HC (9 h light) and normal air (1 and 9 h light, respectively) and compared to each other. Expression analysis was restricted to the protein level, since mRNA levels of photorespiratory genes were found to be unaffected during CO_2 transition (Eisenhut et al., 2016). With regards to mitochondrial photorespiration, we did not observe any major and systematic change in the expression of GDC proteins (P, L and H) or SHMT1 (Supp. Fig. S2). Furthermore, other photorespiratory proteins (PGLP and HPR1) as well as RbcL, the E2 subunits of the oxoglutarate dehydrogenase complex (OGDC) and the pyruvate dehydrogenase complex (PDHC) from the TCA-cycle did also not change in all genotypes at different CO_2 conditions (Supp. Fig. S2). Thus, this experiment demonstrates that neither the knock down of *GDC-T* or the knockout of *TRXo1* alone nor the combination of both alter the abundance of photorespiratory core enzymes during CO_2 transition.

The double mutant *TxGT* exhibits strong impairment of photosynthetic CO_2 assimilation

Given the distinct phenotype of the *TxGT* double mutant, its photosynthetic capacity was next characterized in more detail. Due to the smaller leaves of air-grown *TxGT*, which prevents appropriate gas-exchange measurements, plants were first grown in HC for 7 weeks to synchronize growth. After transfer to normal air and acclimation for 1 week, *gldt1*, *TxGT* and wild-type plants were analyzed. As depicted in Fig. 5, values of A, Γ, oxygen inhibition and γ in wild-type plants are similar to plants consequently grown in normal air (see Fig. 2). However, the *gldt1* mutation has a negative impact on CO_2 assimilation, which steadily increased during measurements with elevated O_2 concentrations. Accordingly, A and Γ of *gldt1* are reduced by about 18% and 14% at low O_2 (3%) but by about 58% and 35% in a high O_2 (50%) atmosphere, respectively (Fig. 5A and C). These changes summed up to an ~80% increase in O_2 inhibition of A and ~116% of γ (Fig. B and C). These alterations are elevated in the *TxGT* plants grown for

one week in normal air. Hence, the decreases in A (~37%) and Γ (~57%) are already larger at low O_2 and significantly higher at 50% O_2 (A - ~83%; Γ - ~86%) (Fig. 5A and C). These inhibitory effects also resulted in increased O_2 inhibition of A (~117%) and enhanced γ (~85%) (Fig. 5B and D). Collectively, these data suggest an additive, negative impact of both mutations on photorespiration, and in turn, photosynthesis.

Impairment of mitochondrial photorespiration alters pyridine nucleotide contents

The above mentioned results provided evidence that *TRXo1* deficiency impacts mitochondrial photorespiration, particularly GDC, known to be the major source of NADH production in illuminated leaves (Leegood et al., 1995). Moreover, TRXo1 belongs to the cellular TRX system which is directly linked to the cellular pyridine nucleotide pools, because NADPH-dependent thioredoxin reductases (NTR) use NADPH as reducing power for various TRX proteins (Geigenberger et al., 2017). Consequently, we next quantified the abundances of pyridine nucleotides (NAD^+, NADH, $NADP^+$ and NADPH) in all genotypes during CO_2 transition. In HC, we did not observe significant alterations in NAD^+, NADH and the NADH/NAD^+ ratio between these genotypes (Fig. 6A, B and C), except a slight increase in the NADH/NAD^+ ratio in the *TxGT* mutant (Fig. 6C). After the transfer to normal air for 1 h, all genotypes display decreased NADH and higher NAD^+ abundances (except *gldt1*), leading to significant reductions in the NADH/NAD^+ ratio in all mutants if compared to the wild type (Fig. 6A, B and C). These changes mostly disappeared after 9 h in normal air, but all mutants consistently showed slightly decreased NADH amounts compared to wild type (Fig. 6A, B and C). Comparable changes were observed in the amounts of the phophorylated pyridine nucleotide abundances. In HC, only the *TxGT* mutant elevated NADPH and decreased $NADP^+$ levels, while the NADPH/$NADP^+$ ratio is higher in the *trxo1* and *TxGT* lines (Fig. 6D, E and F). After the transfer to normal air for 1 as well as 9 h, NADPH is significantly decreased in all genotypes (Fig. 6D), whereas $NADP^+$ is only transiently elevated in *trxo1* and *TxGT* (Fig. 6E). However, all mutant lines are characterized by a significant decrease in the NADPH/$NADP^+$ ratio at both time points in air (Fig. 6F).

The double mutant *TxGT* shows the characteristic photorespiratory metabolic signature

Next we analyzed how the combined mutation of *TRXo1* and *GDC-T* affects the steady-state metabolite profile in *TxGT*. To this end, leaf material from plants grown in either HC (1500 ppm CO_2) or normal air (390 ppm CO_2) was harvested after 9 h of illumination under both conditions and selected metabolites were quantified by LC-MS/MS analysis. As shown in Fig. 7, glycine was invariant between the wild type and *trxo1* in HC, but it already increased in *gldt1* (~1.7-fold) and *TxGT* (~3.5-fold) under this condition. In normal air, leaves of the wild type and the *trxo1*

mutant contain similar amounts of glycine compared to HC. However, a much stronger increase in glycine was observed in leaves of *gldt1* (~17-fold) and especially *TxGT* (~54-fold) under ambient air conditions. These changes, together with the largely unaltered serine amounts in all plant lines, caused also a significant elevation of the cellular glycine-to-serine ratio. Only in *gldt1* and *TxGT* it was already higher at HC (~1.7- and ~2.5-fold) and increased further in normal air (~13.8- and ~43.5-fold) conditions.

Other photorespiratory intermediates did not significantly change between the genotypes after growth in HC, except a slight increase in 3HP in the *TxGT* mutant. Under ambient air conditions, however, we found elevated amounts of glyoxylate (significant in *gldt1* and *TxGT*) and decreased amounts of glycerate (all lines) and 3-PGA (significant in *trxo1* and *TxGT*) in the mutants compared to the wild type (Fig. 7). Only 3HP did not follow this trend given its content was slightly higher in *trxo1* and *TxGT*. The compounds related to redox-homeostasis were also analyzed in this experiment and compared to the results shown in Fig. 2. Except a slight increase in GSH and cysteine in *TxGT*, all three compounds were basically unaltered between the other genotypes and the wild type under HC conditions (Fig. 7). Growth in normal air significantly changed the amounts of all three intermediates. In the wild type, GSH, cysteine and cystine are lower compared to HC (Fig. 7). In the mutants, however, all three intermediates showed gradually increased amounts in the order of their negative impact on photorespiration (*trxo1* < *gldt1* < *TxGT*).

Apart from these changes, several other metabolic alterations previously observed in *trxo1* (Fig. 2, Supp. Table S1) and *gldt1* (Timm et al., 2018) are much more pronounced in the *TxGT* double mutant (Supp. Table S2). For example, *TxGT* accumulates higher amounts of the branched chain amino acids valine (~2.7-fold), isoleucine (~4.2-fold) and leucine (~9.1-fold) as well as the aromatic amino acids phenylalanine (~4.2-fold), tryptophan (~5.5-fold), and tyrosine (~6.6-fold) in normal air compared to the wild type (Fig. 7; Supp. Table 2). Enhanced accumulation was also seen for proline, histidine, arginine, and asparagine, while alanine and aspartate were strongly decreased in *TxGT*. Finally, changes were also observed in the amounts of some TCA-cycle intermediates. For example, malate (~2.0-fold) and citrate (~3.6-fold) were elevated while fumarate (~16% of the wild type) was decreased (Fig. 7; Supp. Table S2). In summary, the combined mutation of *Trxo1* and *GDC-T* enhances the negative impact on GDC activity and causes a metabolic signature comparable to that observed with other mutants showing a strong photorespiratory phenotype (Timm et al., 2012; Eisenhut et al., 2016; Orf et al., 2016; Levey et al., 2018).

Redox-regulation of the GDC L-protein from pea and *Synechocystis* through TRXo1

Given that the GDC expression is unchanged in *trxo1* and the *TxGT* double mutant (see Fig. 2, Supp. Fig. S2), only alterations in the GDC activity could account for the altered glycine accumulation in the mutants. Since H-protein is not enzymatically active and we also observed stronger negative impact on GDC performance in the double mutant with very low GDC-T amounts, we next tested if the GDC-L protein (LPD) activity can be redox-regulated. For this purpose, activity measurements were carried out using LPD from three different sources, namely isolated *Pisum sativum* (pea) leaf-mitochondria (native mtLPD), recombinant mtLPD from pea (*Ps*mtLPD), and recombinant LPD from the cyanobacterium *Synechocystis* PCC 6803 (SyLPD) produced and purified after heterologous expression in *E. coli*. As a representative from a non-photosynthetic organism we further included LPD from *E. coli* for comparison. As shown in Fig. 8, LPD activity from the phototrophic hosts is clearly inhibited upon addition of the artificial reducing agent dithiothreitol (DTT). Its activity decreased to about ~43% (native mtLPD, Fig. 8A), ~52% (*Ps*mtLPD, Fig. 8B) and ~15% (SyLPD, Fig. 8C). Such inhibitory effects were not observed during measurements with *E.coli* LPD (Fig. 8D). Reduction in LPD activity (~35%, ~31% and ~32% for native mtLPD, *Ps*mtLPD and syLPD, respectively) from photosynthetic organisms is also caused through addition of the natural reductant TRXo1 in combination with the NADPH-dependent thioredoxin reductase a (NTRa). Notably, the observed inhibition is due to the activity of the TRXo1/NTRa redox-couple, since no alterations in LPD activity were observed with inactive TRXo1/NTRa (Fig. 8). In summary, these experiments provide evidence that LPD of the plant and cyanobacterial GDC, but not from a heterotrophic organism such as *E. coli*, undergoes redox-regulation.

Finally, to pinpoint critical amino acid residues in the LPD proteins used during this study (pea, Synechocystis and *E. coli*) we analyzed the respective protein sequences in more detail and in comparison to other plant (Arabidopsis, maize) and bacterial (*Azotobacter vinelandii*, *Pseudomonas putida*) representatives. Rationally, the presence of conserved cysteine residues could help to explain a functional mechanism that might involve disulfide bond formation through TRX proteins, presumably TRXo1, in the LPD proteins used during this study (pea, Synechocystis and *E. coli*). All of the analyzed LPD sequences contain two conserved cysteine residues (Cys 45 and Cys 50; Supp. Fig. S3). Previous work has suggested that these residues form a disulfide bond that is involved in FAD-binding and might be of importance for the interaction with the GDC-H protein (Faure et al., 2000). Interestingly, we also found cysteine residues (Cys 34, Cys 335 and Cys 446) that are conserved only in LPD proteins from higher

plants and also in Synechocystis (Cys 34 and Cys 335), but apparently are absent in the proteins from heterotrophic organisms (Supp. Fig. S3). Based on the existing crystal structure of the pea LPD protein (Faure et al., 2000), we generated *in silico* models of the pea, Synechocystis and *E. coli* LPD proteins (Supp. Fig. 4) to find out whether Cys 34, Cys 335 and Cys 446 are in close vicinity in the 3D structure and thus allow disulfide bond formation that could potentially be involved in the redox-regulation of LPDs from photosynthetic organisms. Indeed, all three Cys residues are relatively close to each other between the FAD-binding (Cys 134), the central (Cys 335) and the interface domain (Cys 446). Given that Cys 446 is not present in Synechocystis (redox-regulated), but present in *E. coli* (not redox-regulated), it seems unlikely that this residue is important for activity regulation. Therefore, we conclude that a TRX could potentially form or split a disulfide bond between Cys 34 and Cys 335 to redox-regulate LPD activity.

Discussion

Photorespiration has attracted major interest in plant research and is the currently one of the major targets in plant breeding (Peterhänsel et al., 2013; Betti et al., 2016; Walker et al., 2016; South et al., 2018; 2019). However, regulatory aspects of photorespiration have been only scarcely investigated. To date, no protein with regulatory impact on photorespiration was identified either via classic randomized mutation screens (Somerville, 2001; Badger et al., 2009) or other procedures (Carroll et al., 2015). The failure to identify regulatory candidates by these strategies could be explained by the fact that regulatory mutants might display a rather weak photorespiratory phenotype or that those proteins are often encoded by redundant gene families (Somerville, 2001; Timm and Bauwe, 2013). Nevertheless, there are several hints that some photorespiratory steps such as GDC in the mitochondrion might be prone to redox regulation (Balmer et al., 2004; Keech et al., 2017; Pérez-Pérez et al., 2017). Accordingly, we used a T-DNA insertional mutant that lacks the mitochondrial *TRXo1* (Daloso et al., 2015) to analyze its potential contribution to redox regulation of photorespiration.

TRXo1 contributes to photorespiratory metabolism

The *trxo1* single mutant provides some evidence that this protein could indeed be involved in redox regulation of photorespiration. As such it is perhaps unsurprising that, it shows an increase in the stoichiometry of photorespiratory CO_2 release, which was previously observed also in other mutants with a moderately, constrained photorespiratory flux (Cousins et al., 2011; Timm et al., 2011). Further support that TRXo1 impacts mitochondrial photorespiration was

provided from our metabolite analysis (Fig. 2). Whilst rather minor changes in the glycine-to-serine conversion were observed if *trxo1* was consequently grown in normal air (Fig. 7; Daloso et al., 2015), clear differences in glycine accumulation were found if the mutant was shifted from HC into air to simulate quick photorespiratory activation (Fig. 2). Hence, TRXo1 mediated regulation could play a more dominant role in the short term acclimation of photorespiration to fluctuating environments. In wild-type leaf material, glycine is low under HC conditions but increased about 38-fold after 1 h in LC before it returned to only slightly enhanced levels (~3.8 fold) after 9 h. This strong transient glycine accumulation shortly after induction of photorespiration is consistent with previous reports (Timm et al., 2012; Eisenhut et al., 2016; Orf et al., 2016) and points to the necessity that glycine turnover via GDC needs some activation after HC to LC shifts. Interestingly, such intermittent strong effects on glycine were not found in *trxo1*, here the glycine level rose somewhat continuously from 1 to 9 h in LC. This finding indicates that TRXo1 mediated redox control could somehow inhibit GDC activity in cells grown at HC, which is relieved in the *trxo1* mutant on a short term and in wild type only after longer acclimation to LC conditions. A likely candidate for the TRXo1-mediated redox regulation of GDC is mtLPD since its activity decreases when reduced via this protein (Fig. 8, discussed below in detail). Transient accumulation of the redox-related intermediates GSH, cysteine and cystine in wild-type leaves (Fig. 2) is consistent with the hypothesis that fast HC to LC shifts might result in a transient redox shift in mitochondria, which is lesser pronounced in the *trxo1* mutant. Notably, short term effects on redox-stress intermediates in the wild type can, at least partially, be related to GDC activation. This can be concluded from studies on the *gldt1* mutant, which exhibits an approximate 70% reduction in the total GDC activity (Timm et al., 2018), since it displays increases in these metabolites similar to the wild type after 1 h in LC, but all intermediates do further increase considerably without optimal GDC activity (Fig. 2). Malfunctioning of GDC reduces NADH regeneration and in turn leads to an undersupply of the respiratory chain. This assumption is supported by our quantification of pyridine nucleotide contents during CO_2 transition, which revealed a higher NADH/NAD^+ ratio in the wild type (Fig. 6) in agreement with a higher photorespiratory flux through GDC and thus, increased NADH production. In contrast, impairment of GDC activation/activity in both, *trxo1* and *gldt1*, respectively, causes a distinct drop in the NADH/NAD^+ ratio (Fig. 6). As expected, these effects are mostly seen shortly after HC to ambient air transfer and became somewhat alleviated after 9 h. However, these results provide clear evidence that proper GDC regulation is crucial to maintain the cellular redox-homeostasis. Imbalances of it, particularly in mitochondria, eventually

cause higher production of reactive oxygen species (ROS) that might be counteracted via the accumulated GSH (Fig. 2).

However, the observed effects of the single *TRXo1* mutation on photorespiration and related metabolites are rather weak under standard conditions. Such a behavior has been predicted for other regulatory mutants (Timm and Bauwe, 2013). Moreover, TRXo1 is not the only mitochondrial TRX in Arabidopsis. It is known that TRXh2 is also present in mitochondria (Daloso et al., 2015) and we currently cannot rule out some redundancy between these two proteins, thus weakening the phenotype of single *trxo1* mutant. Given the fact that changes in the phosphorylated pyridine nucleotide contents during CO_2 transition are most dominant in the *trxo1* and *TxGT* mutants shortly after transfer into normal air (Fig. 6D, E and F) it is likely that the decrease of the NADPH/$NADP^+$ ratio can only be partially referred to the feedback inhibition on photosynthesis, particularly the CBC, in response to malfunctioning of photorespiration (Timm et al., 2016). The stronger, intermitted responses in mutants lacking TRXo1 could also lead to activation of other TRX proteins that require a higher NADPH turnover through NTRa. Hence, TRXh2 might, at least to some extent, compensate for the loss of TRXo1 and also act on GDC proteins to regulate their activity. Indeed, similar observations have been made with several TRX target enzymes of the TCA-cycle (Daloso et al., 2015) and future research on multiple mutants is needed to elucidate the interplay between the different TRX proteins and their regulation of GDC.

Lack of *TRXo1* in a *GDC-T* knock down mutant intensifies the photorespiratory phenotype

To further substantiate the impact of TRXo1 on mitochondrial photorespiratory metabolism, we took advantage of a double mutant approach. For this purpose, *trxo1* was crossed into the *gldt1* background, to follow how plant metabolism adapts if overall GDC capacity is decreased to about 70% (*gldt1*; Timm et al., 2018) and additionally lacks the possible TRXo1 mediated redox-regulation. The double mutant *TxGT* showed a more strongly pronounced photorespiratory phenotype than *gldt1.* Growth, PSII activity, and photosynthetic CO_2 assimilation were clearly diminished when cultivated in normal air but remained unaltered if grown in HC (Fig. 4, and 5). These changes provide strong evidence that the *TRXo1* and *GDC-T* mutations are negatively additive for photorespiratory metabolism in mitochondria; i.e. the double mutant *TxGT* clearly amplifies the importance of TRXo1 for photorespiration. This finding could indicate that the absence of TRXo1 further decreases the GDC activity, but not necessarily through affecting the cellular redox-state as evident by the observation that changes in the pyridine nucleotide

contents are similar between the *trxo1* and the *TxGT* mutant (Fig. 6). In this scenario, activity regulation of GDC could occur directly only on GDC-P or GDC-L, since GDC-H is not enzymatically active and GDC-T already highly diminished. This assumption is underpinned by the massive increases in glycine and glycine-to-serine ratio (Fig. 7), indicating intensified impairment of GDC.

The intensified photorespiratory phenotype can potentially also be explained by missing TRXo1-mediated redox regulation of other processes, indirectly affecting the operation of GDC. It has been shown that the *trxo1* mutant exhibits a deregulated TCA cycle (Daloso et al. 2015), which in turn could affect photorespiration due to their physiological interaction (Obata et al., 2016). Changes in TCA cycle intermediates are obvious in the *trxo1* mutant (Supp. Table 1) and are intensified in the case of malate, citrate and fumarate in the *TxGT* double mutant (Supp. Table 2). Moreover, the TRXo1-mediated regulation of mtLPD (Fig. 8) is not only relevant for the regulation of GDC activity, because this protein is also part of the PDHC and OGDC involved in the TCA cycle, as well as the branched-chain 2-oxoacid dehydrogenase complex (BCDHC) involved in the degradation of branch chain amino acid (Oliver et al., 1990; Millar et al., 1998; Timm et al., 2015). Hence, one might speculate that the strongly enhanced photorespiratory phenotype of the *TxGT* plants is partially related to the malfunction of mtLPD in these multiple complexes. Indeed, in support of this theory some characteristic changes in the TCA-cycle and branched chain amino acid metabolism are visible in *trxo1* and *TxGT* under both HC and LC (Supp. Tables 1 and 2).

The above facts notwithstanding, the phenotypic complementation of *TxGT* by elevated CO_2 levels clearly indicates that the main cause of the phenotype is due to a photorespiratory defect. As indicated by the massively elevated glycine amounts this is presumably mediated by an effect on the GDC activity (Fig. 7).

TRXo1 contributes to redox-regulation of GDC through LPD

As mentioned above, all four GDC (P, T, H and L) proteins contain conserved cysteine residues and, thus, were suggested to undergo redox-regulation (Balmer et al., 2004; Keech et al., 2017; Pérez-Pérez et al., 2017). To date, a redox-regulation mechanism was proposed and experimentally verified only for the *Synechocystis* GDC P-protein (Hasse et al., 2013), the actual glycine decarboxylase. It has been also shown that the entire GDC activity became severely inhibited in a more oxidized and ROS producing mitochondrion due to a defect in the ER localized adenylate transporter 1 (*ER-ANT1*) in Arabidopsis and rice (Hoffmann et al., 2013;

Zhang et al., 2016), which was partly relieved upon DTT addition (Hoffman et al., 2013). These findings stimulated us to test GDC-L (mtLPD) for its potential to undergo redox-regulation, which could be based on disulfide bond formation that has been *in silico* predicted onto the LPD structure (Faure et al., 2000). LPD proteins from phototrophic and heterotrophic organisms (Supp. Fig. S3) all possess conserved cys 45 and cys 50 residues that are likely involved in the binding of the FAD-cofactor and interaction with GDC-H (Faure et al., 2000). However, there are other cys residues that are only conserved in LPD proteins from phototrophic organisms, which thus might play a role in TRXo1-based LPD redox-regulation (Supp. Fig. S4). Consistent with this assumption we showed that reducing conditions did not affect LPD from *E. coli* but always inhibited LPD activity from phototrophic origin, including native LPD from pea leaf-mitochondria and recombinant proteins from pea and *Synechocystis* PCC 6803. In addition to DTT, the natural redox-couple consisting of the recombinant mitochondrial TRXo1 and NTRa from Arabidopsis (Reichheld et al., 2007; Daloso et al., 2015) were also able to decrease activity of the plant and cyanobacterial LPD. Redox regulation of LPD has been recently also suggested in experiments to characterize the thioredoxome of Chlamydomonas (Pérez-Pérez et al., 2017). As mentioned before, such a regulation is anticipated to not only affect GDC but also the other mitochondrial enzyme complexes in which LPD is involved in, namely, PDHC, OGDC, as well as BCDHC. Notably, all of the analyzed organic acids involved in the TCA-cycle (malate, citrate, succinate and fumarate) as well as the branched chain (valine, isoleucine and leucine), but not the aromatic (tyrosine, phenylalanine and tryptophane), amino acids essentially show the same accumulation pattern in *trxo1* during HC-to-LC transition as glycine does (Fig. 2, Suppl. Table S1).

The fact that we observed a biphasic response of many metabolites in wild type that was mostly absent in the *trxo1* mutants indicates that redox-regulation occurs on different time scales and might involve other compensatory mechanisms such as through TRXh2. However, our results suggest that TRXo1 is part of the regulation cycle of GDC and the other multi-enzyme systems LPD is involved in. First, and on a shorter time scale (e.g., 1 h after shift to ambient air in our experiment) the presence of TRXo1 (wild-type situation) controls the activation state of LPD and, thus, prevents imbalances in mitochondrial metabolism towards a massive carbon influx into photorespiration that affects the mitochondrial redox-state mainly via elevation of the $NADH/NAD^+$ ratio that in turn would inhibit GDC (Taylor et al., 2002). Given the absence of the strong intermittent glycine accumulation in *trxo1*, it appears that absence of TRXo1 facilitates glycine turnover on the shorter time scale through a more active LPD and, likely, GDC. A similar response was also seen for the intermediates metabolized by PDHC, OGDC, and BCDHC.

Nevertheless, on a longer time scale and also in the *TxGT* double mutant with a "pre-impaired" GDC, absence of TRXo1 no longer facilitates LPD activity. We currently hypothesize that under these conditions another TRX protein, presumably TRXh2, compensates for the lack of TRXo1 to prevent from uncontrolled reduction of NAD^+, as evident from the higher turnover of NADPH in the *trxo1* and the *TxGT* mutant (Fig. 6). Collectively, our results indicate that TRXo1 contributes to the regulation of mitochondrial multi-enzyme systems, particularly GDC, in response to short-term fluctuations caused by environmental changes.

Material and methods

Plant material and growth

Arabidopsis thaliana (Arabidopsis) ecotype Col.0 was used as wild type reference during this study. T-DNA insertional lines *trxo1-1* (SALK 042792) and *gldt1-1* (WiscDSLox 366A11-085) in the Col.0 background were obtained from the Nottingham Arabidopsis Stock Centre (Alonso et al. 2003; Woody et al. 2007) and homozygous lines produced as described previously (Daloso et al., 2015; Timm et al., 2018). After sterilization with chloric acid, seeds were sown on a soil/vermiculite mixture (4:1), incubated at 4°C for 2 days to break dormancy and plants grown under controlled environmental conditions as follows: 10 h day, 20°C/ 14 h night, 18°C, ~ 120 µmol photons m^{-2} s^{-1} light intensity, and 70% relative humidity. Where specified in the text, CO_2 concentration was increased from 390 ppm (normal air) to 1500 ppm (HC - high carbon) with otherwise equal conditions. Plants were regularly watered and fertilized weekly (0.2% Wuxal, Aglukon).

Generation and verification of the *TRXo1* and *GLD-T* double mutant (*TxGT*)

The *trxo1-1* and *gldt1-1* T-DNA insertional lines were crossed to obtain a *trxo1-1*-*gldt1-1* double mutant (*TxGT*). To verify the T-DNA insertions in both genes in the following generations, leaf DNA was isolated according to standard protocols and PCR-amplified (min at 94°C, 1 min at 58°C, 2 min at 72°C; 35 cycles) with primers specific for the left border (R497 for WiscDsLox line, *gldt1-1* or T5 for SALK 042792 line, *trxo1-1*) and *AtGDC-T* (R490) and *TRXo1* (T4) specific primers. The resulting fragments (*gldt1-1* 1859 bp, *trxo1-1* 2000 bp) were sequenced for verification of the T-DNA fragment within both genes. Zygosity was examined by PCR amplification (min at 94°C, 1 min at 58°C, 2 min at 72°C; 35 cycles) of leaf DNA with the primer combination R498 and R490 for *GLD-T* (1943 bp) and T3 and T4 for *TRXo1* (min at 94°C, 1 min at 58°C, 2 min at 72°C; 35 cycles). For oligonucleotide sequences see Supp. Table 3.

qRT-PCR expression analysis and immunological studies

To extract total leaf RNA and protein, plant material (~100 mg) was harvested from air grown wild type and *trxo1-1* plants at growth stage 5.1 (Boyes et al., 2001) after 9 h of illumination or during the CO_2 transfer experiment (Fig. 2) and stored at -80°C until further processing. RNA isolation was carried out using the Nucleospin RNA plant kit (Macherey-Nagel). Following PCR verification of absence of DNA contamination, cDNA was synthesized from 2.5 µg of leaf RNA using the RevertAid cDNA synthesis kit (MBI Fermentas). Prior qRT-PCR analysis cDNA amounts were pre-calibrated by conventional RT-PCR using signals of the constitutively expressed 40S ribosomal protein *S16* gene. qRT-PCR of selected photorespiratory genes (*GLD-P1*, *GLD-T*, *GLD-H*, *GLD-L1*, *SHMT1*, *HPR1*, *pMDH1*, and *PGLP*; for sequences see Supp. Table 3) was performed on the LightCycler 1.5 system (Roche) and SYBR Green fluorescence (Roche) for detection as described previously (Timm et al., 2013). To obtain total leaf-protein, plant material was homogenized and extracted in 200 ml of extraction buffer containing 50 mM HEPES-KOH, pH 7.6, 10 mM NaCl, 5 mM $MgCl_2$, 100 mM sorbitol, and 0.1 mM phenylmethylsulfonyl fluoride. After centrifugation (4°C, 10 min, 20,000*g*), the protein concentration of the supernatant was determined according to Bradford (1976). Subsequently, 10 µg leaf proteins were separated via SDS page and transferred onto a PVDF membrane according to standard protocols. Antibodies of selected photorespiratory proteins (pMDH1, GLD-P, GLD-T, GLD-H, GLD-L, SHMT1, HPR1, and PGLP; Pracharoenwattana et al., 2007; Timm et al., 2013; Flügel et al., 2017) were used to estimate their abundances in the mutant lines and the wild type.

Gas exchange and chlorophyll a fluorescence measurements

Leaf gas exchange measurements were performed using fully expanded rosette leaves of plants at growth stage 5.1 (Boyes et al., 2001) with the following conditions: photon flux density = 1000 µmol m^{-2} s^{-1}, chamber temperature = 25°C, flow rate = 300 µmol s^{-1}, and relative humidity = 60 to 70%. For A/C_i curves CO_2 steps were: 400, 300, 200, 100, 50, 0, and 400 ppm. Changes in the O_2 concentrations to 3, 40 or 50% (balanced with N_2), were generated via the gas-mixing system GMS600 (QCAL Messtechnik). Oxygen inhibition of A was calculated from measurements at 21 and 50% oxygen using the equation: O_2 inhibition = $(A_{21} – A_{50})/A_{21}*100$. Calculation of γ was performed by linear regression of the Γ-versus-oxygen concentration curves and given as slopes of the respective functions. Simultaneously, chlorophyll a fluorescence was determined on a

PAM fluorometer (DUAL-PAM-100; Walz). Maximum quantum yields of PSII were determined after dark adaptation of the plants for at least 15 min.

Metabolite analysis

For LC-MS/MS analysis, leaf material was harvested from fully expanded rosette leaves (sampling time points are specified in the legends of Fig. 2 and 6) of plants at growth stage 5.1 (Boyes et al., 2001), immediately frozen in liquid nitrogen, and stored at -80°C until analysis. Extraction of soluble primary intermediates was carried out using LC-MS grade chemicals according to the method described in Arrivault et al., (2009; 2015) with some modifications. Briefly, ~50 mg leaf-tissue was grounded down to a fine powder and extracted in 500 µl of ice-cold LC-MS/MS buffer (150 µl chloroform, 350 µl methanol, 1 µl of 2-(N-Morpholino)ethanesulfonic acid (MES) as internal standard (1 mg/ml). Following addition of 400 µl ice-cold water samples were vortexed thoroughly and incubated for at least 2 h at -20°C. After centrifugation (10 min, 20000 *g*, 4°C), the aqueous phase was transferred to new tube and 400 µl of ice-cold water again added to the extraction tube. Following stirring and centrifugation (5 min, 20000*g*, 4°C), supernatants were combined and lyophilized. Next, the dried extracts were dissolved in 400 µl water and filtrated through 0.2 µm filters (Omnifix®-F, Braun, Germany). The cleared supernatants were analyzed using the high performance liquid chromatograph mass spectrometer LCMS-8050 system (Shimadzu, Japan) and the incorporated LC-MS/MS method package for primary metabolites (version 2, Shimadzu, Japan). In brief, 1 µl of each extract was separated on a pentafluorophenylpropyl (PFPP) column (Supelco Discovery HS FS, 3 µm, 150 x 2.1 mm) with a mobile phase containing 0.1% formic acid. The compounds were eluted at 0.25 ml min^{-1} using the following gradient: 1 min 0.1% formic acid, 95% *A*. *dest*., 5% acetonitrile, within 15 min linear gradient to 0.1% formic acid, 5% *A*. *dest*., 95% acetonitrile, 10 min 0.1% formic acid, 5% *A*. *dest*., 95% acetonitrile. Aliquots were continuously injected in the MS/MS part and ionized via electrospray ionization (ESI). The compounds were identified and quantified using the multiple reaction monitoring (MRM) values given in the LC-MS/MS method package and the LabSolutions software package (Shimadzu, Japan). Authentic standard substances (Merck, Germany) at varying concentrations were used for calibration and peak areas normalized to signals of the internal standard. Glyoxylate, 3HP and glycerate were determined in the negative ion mode using selective ion monitoring (SIM) for *m/z* 73, 102 and 105 corresponding to the deprotonated glyoxylate, 3HP and glycerate ions $[M-H]^-$. Retention time acquisition window (2 min) was verified with co-elution experiments using purchased glyxoylate, 3HP and glycerate (Sigma-Aldrich, Germany). Varying concentrations of the three metabolites

were also used for calibration curves. Data were interpreted using the Labsolution software package (Shimadzu, Japan).

Determination of pyridine nucleotide contents

The contents of NAD^+/NADH and $NADP^+$/NADPH were determined in acid and alkaline extracts using the protocol described in Queval and Noctor (2007). The assays involve the phenazine methosulfate-catalyzed reduction of dichlorophenolindophenol (DCPIP) in the presence of ethanol and alcohol dehydrogenase (for NAD^+ and NADH) or glucose-6-P and glucose-6-P dehydrogenase (for $NADP^+$ and NADPH). Reduced and oxidized forms are distinguished by preferential destruction through measurements in acid or alkaline buffers.

Cloning, expression and purification of recombinant enzymes

To express bacterial, cyanobacterial and plant LPDs the open reading frames were PCR amplified from *E. coli* genomic DNA (*Ec*LPD; MG1655; *Ec*LPD-S-BamHI/*Ec*LPD-AS-SalI), *Synechocystis* sp. strain PCC 6803 genomic DNA (*Sy*LPD; *slr1096*; 1096XhoI-fw/1096EcoRI-rev) or *Pisum sativum* (*Ps*mtLPD; P454/P294) cDNA and ligated into the pGEMT vector (Invitrogen) for amplification and sequencing (Seqlab, Göttingen). The respective fragments were excised using the introduced restriction sites (*Ec*LPD – BamHI/SalI; *Sy*LPD – XhoI/EcoRI and *Ps*mtLPD – BamHI/EcoRI) and ligated into vector pET28a (Novagene) or pBADHisA (Invitrogen) to obtain pET28a-*Ec*LPD, pBADHisA-*Sy*LPD and pET28a-*Ps*mtLPD. Expression vectors pET16b-*At*TRXo1 and pET16b-*At*NTRa were generated as described previously (Laloi et al., 2001). Overexpression of the 4 constructs was carried out in 200 ml LB-medium containing ampicillin (200 µg mL^{-1}) for the pBADHisA and pET16b or kanamycin (100 µg mL^{-1}) for the pET28a vectors. Overexpression cultures were inoculated with 1 ml of a freshly prepared overnight culture (~16 h) and shaken (200 rpm) at 37°C until OD_{600} = ~0.6. Expression in *Escherichia coli* was carried out as follows: pBADHisA:*Sy*LPD, strain LMG194, induction with 0.2% (w/v) arabinose, and incubation at 30°C (200 rpm) for ~16 h or pET28a and pET16b, strain BL21, induction with IPTG (1 mM), and incubation at 37°C (200 rpm) for 4 h (*Ec*LPD, *At*TRXo1 and *At*NTRa) or 30°C for ~16 h (*Ps*mtLPD1). The cells were harvested and resuspended in 20 mM TrisHCl, pH 8.0, containing 300 mM NaCl, and 20 mM Imidazol. Next, lysozyme was added (1 mg/ml) and the crude extract incubated for 30 min on ice. The proteins were than extracted by ultrasonic treatments (6 x 30 s, 90 W) in ice and centrifugation (20000*g*, 15 min, 4°C). To purify recombinant *Ec*LDP, *Sy*LPD, *Ps*mtLPD, *At*TRXo1 and *At*NTRa, we performed nickel-

nitrilotriacetic acid agarose affinity chromatography according to the protocol of the supplier (HisTrap; GE Healthcare). The eluted proteins were checked regarding purity using SDS-PAGE and staining by Coomassie Brilliant Blue and subsequently used for enzyme measurements.

Isolation of mitochondria and mtLPD activity measurements

To obtain mtLPD for activity measurements, mitochondria were isolated from ~50 g pea leaves according to Keech et al. (2005). Prior activity measurements mitochondria were solubilized by three freeze-thaw cycles, followed by 45 min centrifugation (40000*g*, 4°C). The obtained supernatant was used to determine the protein content. Total mtLPD activity in mitochondrial extracts or of recombinant proteins was assayed spectrophotometrically at 25°C (*Ps*LPD and *Sy*LPD) or 37°C (*Ec*LPD) as described previously (Timm et al., 2015). The reactions were initiated by adding 10-20 µg ml^{-1} mitochondrial or 5-10 µg ml^{-1} recombinant protein. Enzyme activity was determined without (control, oxidizing conditions) or after (reducing conditions) addition with 2 mM dithiothreitol (DTT) for 10 min at room temperature. Furthermore, the artificial proton donor DTT was exchanged with a native mitochondrial redox-system consisting of TRXo1 and NTRa. Briefly, 30 µg NTRa and 12 µg TRXo1 were mixed with 100 µM NADPH in 100 µl potassium-phosphate, incubated for at least 10 min at 25°C and after addition of all other components of the test, mtLPD activity was monitored at 340 nm. For control measurements, the same reactions were carried out after boiling of TRXo1 and NTRa for 10 min at 90°C.

Statistical analysis

Significant values were determined using the two-tailed Student's *t* test (Microsoft Excel 10.0) and by ANOVA for multiple genotypes using the Holm and Sidak test for comparisons (Sigma Plot 11; Systat Software). The term significant is used here only if the change in question has been confirmed to be significant at the level of $*p < 0.05$ or $**p < 0.01$.

Accession numbers

The Arabidopsis Genome Initiative or GenBank/EMBL database contains sequence data from this article under the following accession numbers: TRXo1 (At2g35010), NTRa (At2g17420), GDC-T (At1g11680), GDC-P1 (At4g33010), GDC-H1 (At1g32470), GDC-L1 (mtLPD1) (At1g48030), GDC-L2 (AT3G17240), SHMT1 (At4g37930), pMDH (At2g22780), HPR1 (At1g68010), PGLP1 (At5g35700), ODGC-E2 (At5g55070), PDC-E2 (At3g52200), RbcL (ATCG00490), 40S ribosomal protein S16 (At2g09990), pea LPD (P31023), maize LPD

(A0A1D6MSE3), Syn LPD (P72740), *E.coli* LPD (P0A9P0), *Azotobacter vinelandii* LPD (C1DGW2) and *Pseudomonas putida* LPD (Q88C17).

Author Contributions

S.T. conceived and supervised the project. O.R., S.S., Y.Z. and S.T. performed the research and analyzed data. J.P.R. provided expression clones for TRXo1 and NTRa and A.R.F. the T-DNA insertional mutant *trxo1-1*. A.R.F. and M.H. provided experimental equipment and tools. S.T. wrote the article, with additions and revisions from all authors. All authors have read and approved the final version of the manuscript.

Acknowledgements

We wish to thank Maria Wittmiß (Rostock) for introducing O.R. in enzymatic measurements and providing recombinant LPD of Synechocystis PCC6803 and the Nottingham Arabidopsis Stock Centre for the T-DNA insertional lines. We also acknowledge the technical assistance from Ina Krahnert (Potsdam-Golm). The donation of antibodies received from Hermann Bauwe (University of Rostock, Germany) and Steven M. Smith (University of Tasmania, Australia) has facilitated the study. This work was financially supported by the University of Rostock (to M.H. and S.T.). The LC-MS equipment at the University of Rostock was financed through the HBFG program (GZ: INST 264/125-1 FUGG). This study is set within the framework of the "Laboratoires d'Excellences (LABEX)" TULIP (ANR-10-LABX-41).

Supplemental Data

Supplemental Table 1. Absolute metabolite contents in *trxo1* and the wild type during CO_2 transition.

Supplemental Table 2. Absolute metabolite contents in *trxo1*, *gldt1* and *TxGT* compared to the wild type grown in HC and LC conditions.

Supplemental Table 3. Oligonucleotides used during this study.

Supplemental Figure 1. Phenotype and PCR verification of the *TxGT* double mutant.

Supplemental Figure 2. Expression of selected photorespiratory and TCA cycle enzymes during CO_2 transition.

Supplemental Figure 3. Alignment of LPD proteins from different sources.

Supplemental Figure 4. 3D protein structure models of pea, Synechocystis and *E.coli* LPD.

693

694**1**

695**2**

Literature cited

Alonso JM, Stepanova AN, Leisse TJ, Kim CJ, Chen H, Shinn P, Stevenson DK, Zimmerman J, Barajas P, Cheuk R, Gadrinab C, Heller C, Jeske A, Koesema E, Meyers CC, Parker H, Prednis L, Ansari Y, Choy N, Deen H, Geralt M, Hazari N, Hom E, Karnes M, Mulholland C, Ndubaku R, Schmidt I, Guzman P, Aguilar-Henonin L, Schmid M, Weigel D, Carter DE, Marchand T, Risseeuw E, Brogden D, Zeko A, Crosby WL, Berry CC, Ecker JR (2003) Genome-wide insertional mutagenesis of *Arabidopsis thaliana*. Science **301:** 653-657

Anderson LE (1971) Chloroplast and cytoplasmic enzymes. II. Pea leaf triose phosphate isomerases. Biochimmica et Biophysica Acta **235:** 237–244

Appel AM, Bercaw JE, Bocarsly AB, Dobbek H, DuBois DL, Dupuis M, Ferry JG, Fujita E, Hille R, Kenis PJA, Kerfeld CA, Morris RH, Peden CHF, Portis AR, Ragsdale SW, Rauchfuss TB, Reek JNH, Seefeldt LC, Thauer RK, Waldrop GL. (2013) Frontiers, Opportunities, and Challenges in Biochemical and Chemical Catalysis of CO_2 Fixation. Chemical Reviews **113:** 6621-6658

Arrivault S, Guenther M, Ivakov A, Feil R, Vosloh D, van Dongen JT, Sulpice R, Stitt M (2009) Use of reverse-phase liquid chromatography, linked to tandem mass spectrometry, to profile the Calvin cycle and other metabolic intermediates in Arabidopsis rosettes at different carbon dioxide concentrations. Plant Journal **5:** 826–39

Arrivault, S, Guenther, M, Fry, SC, Fuenfgeld, MMFF, Veyel, D, Mettler-Altmann, T, Stitt, M, Lunn, JE (2015) Synthesis and use of stable-isotope-labeled internal standards for quantification of phosphorylated metabolites by LC-MS/MS. Analytical Chemistry **87:** 6896–6904.

Badger MR, Fallahi H, Kaines S, Takahashi S (2009) Chlorophyll fluorescence screening of *Arabidopsis thaliana* for CO_2 sensitive photorespiration and photoinhibition mutants. Functional Plant Biology **36:** 867-873

Balmer Y, Vensel WH, Tanaka CK, Hurkman WJ, Gelhaye E, Rouhier N, Jacquot JP, Manieri W, Schürmann P, Droux M, Buchanan B (2004) Thioredoxin links redox to the regulation of fundamental processes of plant mitochondria. Proc. Natl. Acad. Sci. USA **101:** 2642–2647

Bauwe H, Hagemann M, Fernie AR (2010) Photorespiration: players, partners and origin. Trends in Plant Science **15:** 330-336

Bauwe H, Hagemann M, Kern R, Timm S (2012) Photorespiration has a dual origin and manifold links to central metabolism. Current Opinion in Plant Biology **15:** 269-275

Betti M, Bauwe H, Busch FA, Fernie AR, Keech O, Levey M, Ort DR, Parry MAJ, Sage R, Timm S, Walker B, Weber APM (2016) Manipulating photorespiration to increase plant productivity: recent advances and perspectives for crop improvement. Journal of Experimental Botany **67:** 2977-2988

Blackwell RD, Murray AJS, Lea PJ, Kendall AC, Hall NP, Turner JC, Wallsgrove RM (1988) The value of mutants unable to carry out photorespiration. Photosynthesis Research **16:** 155-176

Bradford MM (1976) A rapid and sensitive method for the quantitation of microgram quantities of protein utilizing the principle of protein-dye binding. Anal Biochem **72:** 248–254

Bourguignon J, Neuburger M, Douce R (1988) Resolution and characterization of the glycine cleavage reaction in pea leaf mitochondria. Properties of the forward reaction catalysed by glycine decarboxylase and serine hydroxymethyltransferase. Biochemical Journal **255:** 169-78

Bowes G, Ogren WL, Hageman RH (1971) Phosphoglycolate production catazyded by ribulose diphosphate carboxylase. Biochemical and Biophysical Research Communications **45:** 716-722

Boyes DC, Zayed AM, Ascenzi R, McCaskill AJ, Hoffman NE, Davis KR, Gorlach J (2001) Growth stage-based phenotypic analysis of Arabidopsis: A model for high throughput functional genomics in plants. Plant Cell **13:** 1499-1510

Carroll AJ, Zhang P, Withehead L, Kaines S, Tcherkez G, Badger MJ (2015) PhenoMeter: a metabolome database search tool using statistical similarity matching of metabolic phenotypes for high-confidence detection of functional links. Frontiers in Bioengineering and Biotechnology https://doi.org/10.3389/fbioe.2015.00106

Cousins AB, Walker BJ, Pracharoenwattana I, Smith SM, Badger MR (2011) Peroxisomal hydroxypyruvate reductase is not essential for photorespiration in Arabidopsis but its absence causes an increase in the stoichiometry of photorespiratory CO_2 release. Photosynthesis Research **108:** 91-100

Daloso, DM, Müller K, Obata T, Florian A, Tohge T, Bottcher A, Riondet C, Bariat L, Carrari F, Nunes-Nesi A, Buchanan BB, Reichheld J-P, Araújo WL, Fernie AR (2015) Thioredoxin, a master regulator of the tricarboxylic acid cycle in plant mitochondria. Proceedings of the National Academy of Sciences of the United States of America, **112:** 1392-1400

Dellero Y, Lamothe-Sibold M, Jossier M, Hodges M (2015) Arabidopsis thaliana ggt1 photorespiratory mutants maintain leaf carbon:nitrogen balance by reducing RuBisCO content and plant growth. The Plant Journal **83:** 1005-1018

Douce R, Bourguignon J, Besson V, Macherel D, Neuburger M (1991) Structure and function of the glycine cleavage complex in green leaves. In: Huang AHC, Taiz L, eds. Molecular approaches to compartmentation and metabolic regulation. Rockville: American Society of Plant Physiologists, 59-73.

Douce R, Bourguignon J, Neuburger M, Rébeillé F (2001) The glycine decarboxylase system: a fascinating complex. Trends Plant Science **6:** 167–176

Eisenhut M, Ruth W, Haimovich M, Bauwe H, Kaplan A, Hagemann M (2008) The photorespiratory glycolate metabolism is essential for cyanobacteria and might have been conveyed endosymbiontically to plants. Proceedings of the National Academy of Sciences, USA **105:** 17199–17204

Eisenhut M, Planchais S, Cabassa C et al. (2013a) Arabidopsis A BOUT DE SOUFFLE is a putative mitochondrial transporter involved in photorespiratory metabolism and is required for meristem growth at ambient CO_2 levels. The Plant Journal **73:** 836-849

Eisenhut M, Bräutigam A, Timm S, Florian A, Tohge T, Fernie AR, Bauwe H, Weber A (2016) Photorespiration is crucial to the dynamic response of photosynthetic metabolism to altered CO_2 availability. Molecular Plant **10:** 47-61

Faure M, Bourguingnon J, Neuburger M, MacHerel D, Sieker L, Ober R, Kahn R, Cohen-Addad C, Douce R (2000) Interaction between the lipoamide-containing H-protein and the lipoamide dehydrogenase (L-protein) of the glycine decarboxylase multienzyme system 2. Crystal structures of H- and L-proteins. Eur. J. Biochem. **267:** 2890-2898

Fernie A, Bauwe H, Eisenhut M, Florian A, Hanson D, Hagemann M, Keech O, Mielewczik M, Nikoloski Z, Peterhänsel C, Roje S, Sage R, Timm S, von Caemmerer S, Weber A,

Westhoff P (2013) Perspectives on plant photorespiratory metabolism. Plant Biology **45:** 748-753

Flügel F, Timm S, Arrivault S, Florian A, Stitt M, Fernie AR, Bauwe H (2017) The Photorespiratory Metabolite 2-Phosphoglycolate Regulates Photosynthesis and Starch Accumulation in Arabidopsis. The Plant Cell **29:** 2537-2551

Foyer CH, Bloom AJ, Queval G, Noctor G (2009) Photorespiratory metabolism: genes, mutants, energetics, and redox signaling. Annual Reviews in Plant Biology **60:** 455-484

Geigenberger P, Thormählen I, Daloso DM, Fernie A.R. (2017) The unprecedented versatility of the plant thioredoxin system. Trends in Plant Science **22:** 249–262

Hasse D, Andersson E, Carlsson G, Masloboy A, Hagemann M, Bauwe H, Andersson I (2013) Structure of the homodimeric glycine decarboxylase P-protein from Synechocystis sp. PCC 6803 suggests a mechanism for redox regulation. Journal of Biological Chemistry **288:** 35333-35345

Hodges M, Jossier M, Boex-Fontvieille E, Tcherkez G (2013) Protein phosphorylation and photorespiration. Plant Biology **15:** 694–706

Hodges M, Dellero Y, Keech O, Betti M, Raghavendra AS, Sage R, Zhu XG, Allen DK, Weber AP (2016) Perspectives for a better understanding of the metabolic integration of photorespiration within a complex plant primary metabolism network. Journal of Experimental Botany **67:** 3015–3026

Hodges M, Jossier M, Boex-Fontvieille E, Tcherkez G (2013) Protein phosphorylation and photorespiration. Plant Biology **15:** 694–706

Hoffmann C, Plocharski B, Haferkamp I, Leroch M, Ewald R, Bauwe H, Riemer J, Herrmann J, Neuhaus E (2013) From endoplasmic reticulum to mitochondria: Absence of the Arabidopsis ATP antiporter ER-ANT1 perturbs photorespiration. The Plant Cell **25:** 2647-2660

Keech O, Dizengremel P, Gardeström P (2005) Preparation of leaf mitochondria from Arabidopsis thaliana. Physiol Plant **124:** 403–409

Keech O, Gardeström P, Kleczskowski LA, Rouhier N (2017) The redox control of photorespiration: from biochemical and physiological aspects to biotechnological considerations. Plant Cell Environment **40:** 553-569

Kelly GJ, Latzko E (1976) Inhibition of spinach-leaf phosphofructokinase by 2-phosphoglycollate. FEBS Letters **68:** 55–58

Laloi C, Rayapuram N, Chartier Y, Grienenberger JM, Bonnar G, Meyer Y (2001) Identification and characterization of a mitochondrial thioredoxin system in plants. Proceedings of the National Academy of Sciences of the United States of America, 98: 14144-14149

Li J, Weraduwage SM, Peiser AL, Tietz S, Weise SE, Strand DD, Froehlich JE, Kramer DM, Hu J, Sharkey TD (2019) A Cytosolic Bypass and G6P Shunt in Plants Lacking Peroxisomal Hydroxypyruvate Reductase. Plant Physiology DOI:https://doi.org/10.1104/pp.19.00256

Leegood RC, Lea PJ, Adcock MD, Häusler RE (1995) The regulation and control of photorespiration. Journal of Experimental Botany **46:** 1397-1414

Levey M, Timm S, Mettler-Altmann T, Borghi GL, Koczor M, Arrivault S, Weber APM, Bauwe H, Gowik U, Westhoff P (2019) Efficient 2-phosphoglycolate degradation is required to maintain carbon assimilation and allocation in the C_4 plant *Flaveria bidentis*. Journal of Experimental Botany, **70:** 575-587

López-Calcagno PE, Fisk S, Brown KL, Bull SE, South PF, Raines CA (2018) Overexpressing the H-protein of the glycine cleavage system increases biomass yield in glasshouse and field-grown transgenic tobacco plants. Plant Biotechnology Journal doi: 10.1111/pbi.12953

Millar AH, Knorpp C, Leaver CJ, Hill SA (1998) Plant mitochondrial pyruvate dehydrogenase complex: purification and identification of catalytic components in potato. Biochemical Journal **334:** 571–576

Nakamura Y, Kanakagiri S, Van K, He W, Spalding MH (2005) Disruption of the glycolate dehydrogenase gene in the high-CO2-requiring mutant HCR89 of Chlamydomonas reinhardtii. Canadian Journal of Botany **83:** 820–833

Obata T, Florian A, Timm S, Bauwe H, Fernie AR (2016) On the metabolic interaction of (photo)respiration. Journal of Experimental Botany **67:** 3003-3014

Ogren WL, Bowes G (1971) Ribulose diphosphate carboxylase regulates soybean photorespiration. Nature New Biology **230:** 159–160

Oliver DJ, Sarojini G (1987) Regulation of glycine decarboxylase by serine. In: Biggins J, ed. Progress in photosynthesis research, Vol. III. Dordrecht: Martinus Nijhoff, 573-6.

Oliver DJ, Neuburger M, Bourguignon J, Douce R (1990) Interaction between the component enzymes of the glycine decarboxylase multienzyme complex. Plant Physiology **94:** 833–839

Orf I, Timm S, Bauwe H, Fernie AR, Hagemann M, Kopka J, Nikoloski Z (2016) Can cyanobacteria serve as a model of plant photorespiration? – A comparative analysis of metabolite profiles. Journal of Experimental Botany **67:** 2941-2952

Palmieri MC, Lindermayr C, Bauwe H, Steinhauser C, Durner J (2010) Regulation of Plant Glycine Decarboxylase by *S*-Nitrosylation and Glutathionylation. Plant Physiology **152:** 1514-1528

Peterhänsel C, Krause K, Braun H-P, Espie GS, Fernie AR, Hanson DT, Keech O, Maurino VG, Mielewczik M, Sage RF (2013) Engineering photorespiration: current state and future possibilities. Plant Biology **15:** 754–758

Pérez-Pérez ME, Mauriès A, Maes A, Tourasse NJ, Hamon M, Lemaire SD, et al. (2017) The deep thioredoxome in *Chlamydomonas reinhardtii*: new insights into redox regulation. Molecular Plant **10:** 1107–1125

Pick TR, Bräutigam A, Schulz MA, Obata T, Fernie AR, Weber APM (2013) PLGG1, a plastidic glycolate glycerate transporter, is required for photorespiration and defines a unique class of metabolite transporters. Proceedings of the National Academy of Sciences of the United States of America **110:** 3185-3190

Pracharoenwattana I, Cornah JE, Smith SM (2007) Arabidopsis peroxisomal malate dehydrogenase functions in β-oxidation but not in the glyoxylate cycle. The Plant Journal, **50:** 381-390

Queval G, Noctor G (2007) A plate reader method for the measurement of NAD, NADP, glutathione, and ascorbate in tissue extracts: application to redox profiling during Arabidopsis rosette development. Anal Biochem **363:** 58–69

Rademacher N, Kern R, Fujiwara T, Mettler-Altmann T, Miyagishima SY, Hagemann M, Eisenhut M, Weber AP (2016) Photorespiratory glycolate oxidase is essential for the survival of the red alga Cyanidioschyzon merolae under ambient CO_2 conditions. Journal of Experimental Botany **67:** 3165–3175

Reichheld JP, Khafif M, Riondet C, Droux M, Bonnard G, Meyer Y (2007) Inactivation of thioredoxin reductases reveals a complex interplay between thioredoxin and gluthatione pathways in Arabidopsis development. Plant Cell **19:** 1851-1865

Reumann S, Weber APM (2006) Plant peroxisomes respire in the light: Some gaps of the photorespiratory C2-cycle have becomes filled – Others remain. Biochimica et Biophysica Acta **1763:** 1496-1510

Simkin A, Lopez-Calcagno P, Davey P, Headland L, Lawson T, Timm S, Bauwe H, Raines C (2017) Simultaneous stimulation of the SBPase, FBP aldolase and the photorespiratory GDC-H protein increases CO_2 assimilation, vegetative biomass and seed yield in Arabidopsis. Plant Biotechnology Journal **15:** 805-816

Somerville CR (2001) An early Arabidopsis demonstration. Resolving a few issues concerning photorespiration. Plant Physiology **125:** 20–24

Somerville CR, Ogren WL (1979) Phosphoglycolate phosphatase-deficient mutant of Arabidopsis. Nature **280:** 833-836

South PF, Cavanagh AP, Lopez-Calcagno PE, Raines CA, Ort DR (2018) Optimizing photorespiration for improved crop productivity. Journal of Integrative Plant Biology doi: 10.1111/jipb.12709

South PF, Cavanagh AP, Liu HW, Ort DR (2019) Synthetic glycolate metabolism pathways stimulate crop growth and productivity in the field. Science **363** (6422). doi: 10.1126/science.aat9077

Suzuki K, Marek LF, Spalding MH (1989) A photorespiratory mutant of Chlamydomonas reinhardtii. Plant Physiology **93:** 231–237

Taylor NL, Day DA, Millar AH (2002) Environmental stress causes oxidative damage to plant mitochondria leading to inhibition of glycine decarboxylase. The Journal of Biological Chemistry **277:** 42663–42668

Timm S, Florian A, Jahnke K, Nunes-Nesi A, Fernie AR, Bauwe H (2011) The hydroxypyruvate-reducing system in Arabidopsis: multiple enzymes for the same end. Plant Physiology **155:** 694–705

Timm S, Mielewczik M, Florian A, Frankenbach S, Dreissen A, Hocken N, Fernie AR, Walter A, Bauwe H (2012a) High-to-low CO_2 acclimation reveals plasticity of the photorespiratory pathway and indicates regulatory links to cellular metabolism of Arabidopsis. PLoS ONE 7, e42809.

Timm S, Florian A, Arrivault S, Stitt M, Fernie AR, Bauwe H (2012b) Glycine decarboxylase controls photosynthesis and plant growth. FEBS Letters **586:** 3692-3697

Timm S, Bauwe H (2013) The variety of photorespiratory phenotypes - employing the current status for future research directions on photorespiration. Plant Biology **15:** 737-747**.**

Timm S, Florian A, Wittmiß M, Jahnke K, Hagemann M, Fernie AR, Bauwe H (2013) Serine acts as metabolic signal for the transcriptional control of photorespiration-related genes in *Arabidopsis thaliana*. Plant Physiology **162:** 379-389

Timm S, Wittmiß M, Gamlien S, Ewald R, Florian A, Frank M, Wirtz M, Hell R, Fernie AR, Bauwe H (2015) Mitochondrial dihydrolipoyl dehydrogenase activity shapes photosynthesis and photorespiration of *Arabidopsis thaliana*. The Plant Cell **27:** 1968-1984

Timm S, Florian A, Fernie AR, Bauwe H (2016) The regulatory interplay between photorespiration and photosynthesis. Journal of Experimental Botany **67:** 2923-2929

Timm S, Giese J, Engel N, Wittmiß M, Florian A, Fernie AR, Bauwe H (2018) T-protein is present in large excess over the other proteins of the glycine cleavage system in leaves of Arabidopsis. Planta **1:** 41-51

Tolbert NE (1971) Microbodies Peroxisomes and glyoxysomes. Annual Reviews in Plant Physiology **22:** 45–74

Walker JL, Oliver DJ (1986) Light-induced increases in the glycine decarboxylase multienzyme complex from pea leaf mitochondria. Archives of Biochemistry and Biophysics **248:** 626-638

Walker BJ, VanLoocke A, Bernacchi CJ, Ort DR (2016) The costs of photorespiration to food production now and in the future. Annual Review of Plant Biology **67:** 107- 129

Wingler A, Lea PJ, Quick WP, Leegood RC (2000) Photorespiration: metabolic pathways and their role in stress protection. Philos. Trans. R. Soc. London Ser. B **355:** 1517–29

Woody ST, Austin-Phillips S, Amasino RM, Krysan PJ (2007) The *WiscDsLox* T-DNA collection: an arabidopsis community resource generated by using an improved high-throughput T-DNA sequencing pipeline. J Plant Res **120:** 157-165

Vauclare P, Diallo N, Bourguignon J, Macherel D, Douce R (1996) Regulation of the Expression of the Glycine Decarboxylase Complex during Pea Leaf Development. Plant Physiology **112:** 1523-1530

Zelitch I (1964) Organic acids and respiration in photosynthetic tissues. Annual Reviews in Plant Physiology **15:** 121–142

Zelitch I, Schultes NP, Peterson RB, Brown P, Brutnell TP (2009) High glycolate oxidase activity is required for survival of maize in normal air. Plant Physiology **149:** 195–204

Zhang X, Zheng X, Ke S, Zhu H, Liu F, Zhang Z, Peng X, Guo L, Zeng R, Hou P, Liu Z, Wu S, Song M, Yang J, Zhang G (2016) ER-localized adenine nucleotide transporter ER-ANT1: an integrator of energy and stress signaling in rice. Plant Molecular Biology **92:** 701-715

Figure legends

Figure 1. Oxygen-dependent gas exchange of *trxo1* and the wild type.

Plants were grown in normal air (390 ppm CO_2) with a 10/14 h day/night cycle. After 8 weeks (growth stage 5.1, Boyes et al., 2001), plants were used for gas exchange measurements at varying oxygen concentrations (3%, 21%, 40%, and 50%, balanced with N_2). Mean values ± SD (n = 5-8) are shown for **(A)** net CO_2 uptake rates (A) and oxygen inhibition of A and **(B)** CO_2 compensation points (Γ) and slopes of the Γ-versus-oxygen concentrations (γ). Asterisks indicate significant alterations of the *trxo1* mutant to the wild type according to Student's *t*-test (*p < 0.05, **p < 0.01, n.s. – not significant). For details on the calculation of oxygen inhibition and γ see material and methods section.

Figure 2. Selected metabolites in wild type, *trxo1* and *gldt1* plants during CO_2 transition.

Plants were grown in high CO_2 (1500 ppm, HC) with a 10/14 h day/night cycle. After 8 weeks (growth stage 5.1, Boyes et al., 2001) plants were transferred in normal air (390 CO_2) with otherwise equal conditions. Leaf-material was harvested in HC (9 h light) and in normal air (1 and 9 h light), respectively. Shown are mean values ± SD (n = 6) of selected metabolites quantified by LC-MS/MS analysis. For a more comprehensive dataset including statistical evaluation please compare Supp. Datasheet 1.

Figure 3. Expression of selected photorespiratory enzymes on the mRNA and protein level.

Plants were grown in normal air (390 ppm CO_2) with a 10/14 h day/night cycle. After 8 weeks (growth stage 5.1, Boyes et al., 2001), leaf-material was harvested at the end of the day (9 h illumination) and used for subsequent mRNA and protein extraction. Shown are mean values ± SD (n = 3) of mRNA expression and representative immunoblots from the *trxo1* mutant compared to the control (n.s. – not significant; n.d. – not determined).

Figure 4. Phenotype, growth and chlorophyll a fluorescence of the *TxGT* double mutant.

Plants were grown in **(A)** normal air (390 ppm CO_2) or **(B)** high CO_2 (1500 ppm, HC) with a 10/14 h day/night cycle. After 5 weeks plants were photographed, rosette diameters and total leaf-numbers determined and chl a fluorescence measurements carried out. Shown are mean values ± SD (n > 5). Asterisks indicate values significantly different from the control (*p < 0.05;

**p < 0.01; n.s. – not significant) and plusses between the *gldt1* single and the *TxGT* double mutant ($^{+}$p < 0.05).

Figure 5. Oxygen-dependent gas exchange of *gldt1*, *TxGT* and the wild type.

Plants were grown in high CO_2 (1500 ppm) with a 10/14 h day/night cycle. After 7 weeks (growth stage 5.1, Boyes et al., 2001), plants were transferred to normal air (390 ppm CO_2) and used for gas exchange measurements at varying oxygen concentrations (3%, 21%, and 50%, balanced with N_2) after one week acclimation to the altered atmosphere. Mean values ± SD (n = 5-8) are shown for **(A)** net CO_2 uptake rates (A) and oxygen inhibition of A and **(B)** CO_2 compensation points (Γ) and slopes of the Γ-versus-oxygen concentrations (γ). Asterisks indicate significant alterations of the mutants to the wild type according to Student's *t*-test (*p < 0.05, **p < 0.01) and plusses between the *gldt1* single and the *TxGT* double mutant ($^{+}$p < 0.05). For details on the calculation of oxygen inhibition and γ see material and methods section.

Figure 6. Pyridine nucleotide contents in wild type, *gldt1*, *trxo1* and *TxGT* plants during CO_2 transition.

Plants were grown in high CO_2 (1500 ppm, HC) with a 10/14 h day/night cycle. After 8 weeks (growth stage 5.1, Boyes et al., 2001) plants were transferred in normal air (390 ppm CO_2) with otherwise equal conditions. Leaf-material was harvested in HC (9 h light) and in normal air (1 and 9 h light), respectively. Shown are mean values ± SD (n > 6) of pyridine nucleotides (NAD^+, NADH, $NADP^+$ and NADPH) quantified by spectrophotometric analysis. Asterisks indicate significant alterations of the mutants to the wild type according to Student's *t*-test (*p < 0.05, **p < 0.01, n.s. – not significant).

Figure 7. Levels of selected metabolites in leaves of the wild type, *trxo1*, *gldt1* and *TxGT* mutants grown in HC and normal air.

Plants were grown in high CO_2 (1500 ppm, HC) and normal air (390 ppm CO_2) with a 10/14 h day/night cycle. After 8 weeks (growth stage 5.1, Boyes et al., 2001), leaf-material was harvested in both conditions after 9 h illumination. Shown are mean values ± SD (n > 4) of selected metabolites quantified by LC-MS/MS analysis. Asterisks indicate significant alterations of the mutants to the wild type in each condition according to Student's *t*-test (*p<0.05; **p<0.01) and plusses between HC and normal air values of each genotype (*p<0.05). For a more comprehensive dataset including statistical evaluation please compare Supp. Datasheet 2.

Figure 8. Redox-regulation of mtLPD1 from pea and Synechocystis.

The activity of mtLPD was determined in **(A)** pea leaf-mitochondria and from recombinant **(B)** pea and **(C)** Synechocystis proteins, respectively. Shown are mean values ± SD (n > 4) of mtLPD activity without or after addition of DTT and recombinant native or boiled TRXo1 and NTRa as described in detail in the material and methods section. Asterisks indicate significant alterations to the control according to Student's *t*-test (*p < 0.05, **p < 0.01, n.s. – not significant).

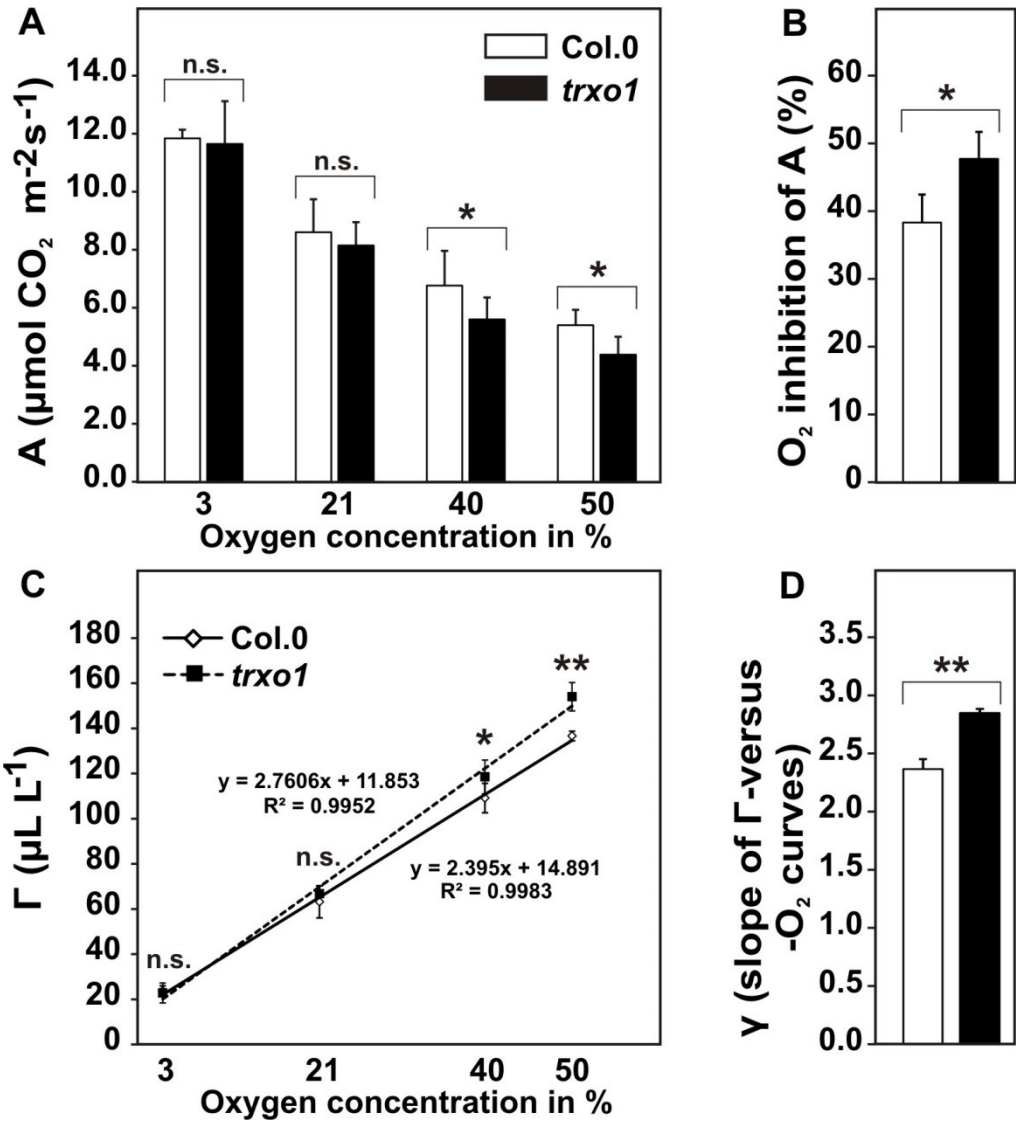


Figure 1. Oxygen-dependent gas exchange of *trxo1* and the wild type.

Plants were grown in normal air (390 ppm CO_2) with a 10/14 h day/night cycle. After 8 weeks (growth stage 5.1, Boyes et al., 2001), plants were used for gas exchange measurements at varying oxygen concentrations (3%, 21%, 40%, and 50%, balanced with N_2). Mean values ± SD (n = 5-8) are shown for **(A)** net CO_2 uptake rates (A) and **(B)** oxygen inhibition of A and **(C)** CO_2 compensation points (Γ) and **(D)** slopes of the Γ-versus-oxygen concentrations (γ). Asterisks indicate significant alterations of the *trxo1* mutant to the wild type according to Student's *t*-test (*p < 0.05, **p < 0.01, n.s. – not significant). For details on the calculation of oxygen inhibition and γ see material and methods section.

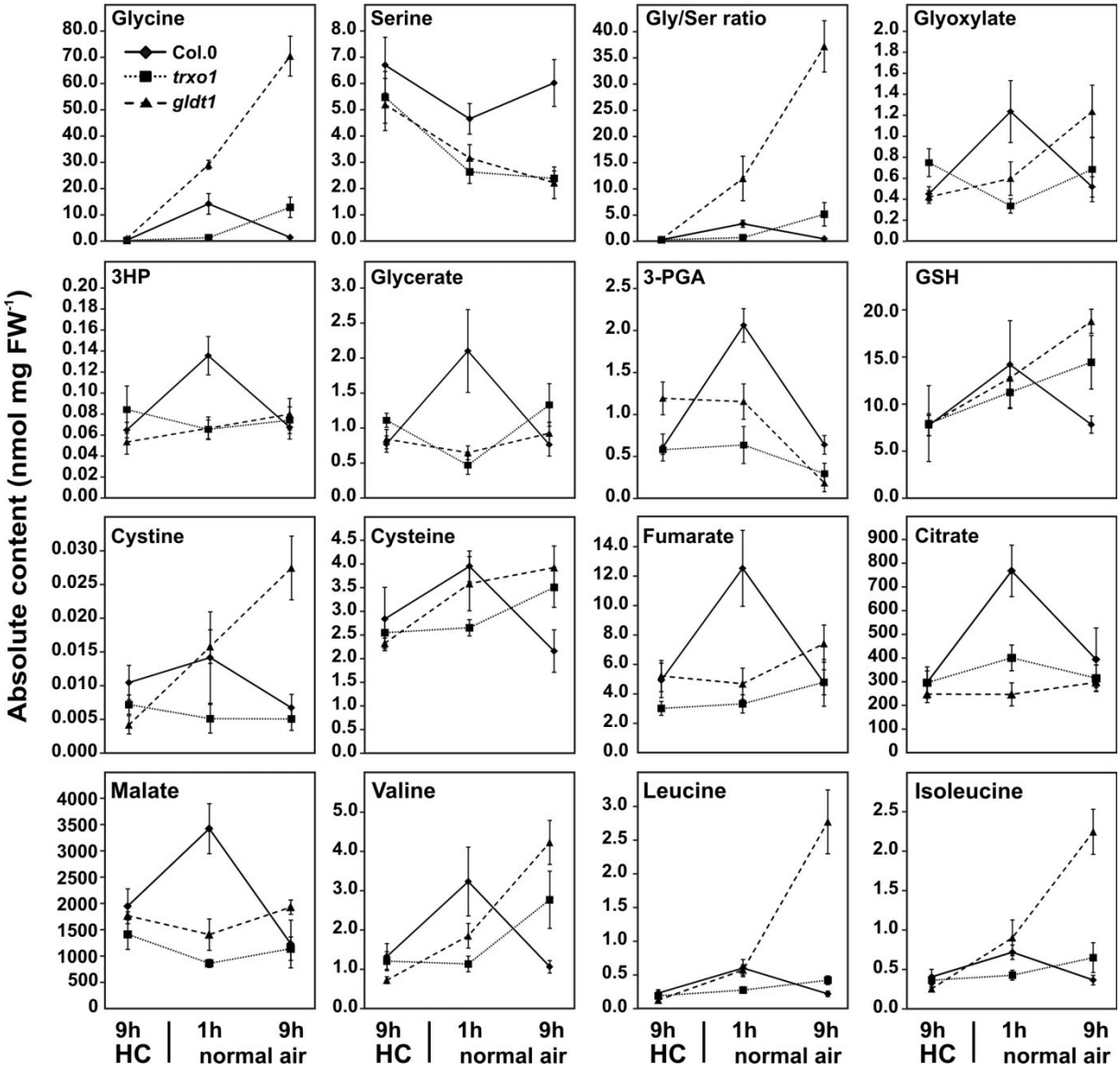


Figure 2. Selected metabolites in wild type, *trxo1* and *gldt1* plants during CO_2 transition.

Plants were grown in high CO_2 (1500 ppm, HC) with a 10/14 h day/night cycle. After 8 weeks (growth stage 5.1, Boyes et al., 2001) plants were transferred in normal air (390 CO_2) with otherwise equal conditions. Leaf-material was harvested in HC (9 h light) and in normal air (1 and 9 h light), respectively. Shown are mean values ± SD (n = 6) of selected metabolites quantified by LC-MS/MS analysis. For the full dataset including statistical evaluation please compare Supp. Table 1.

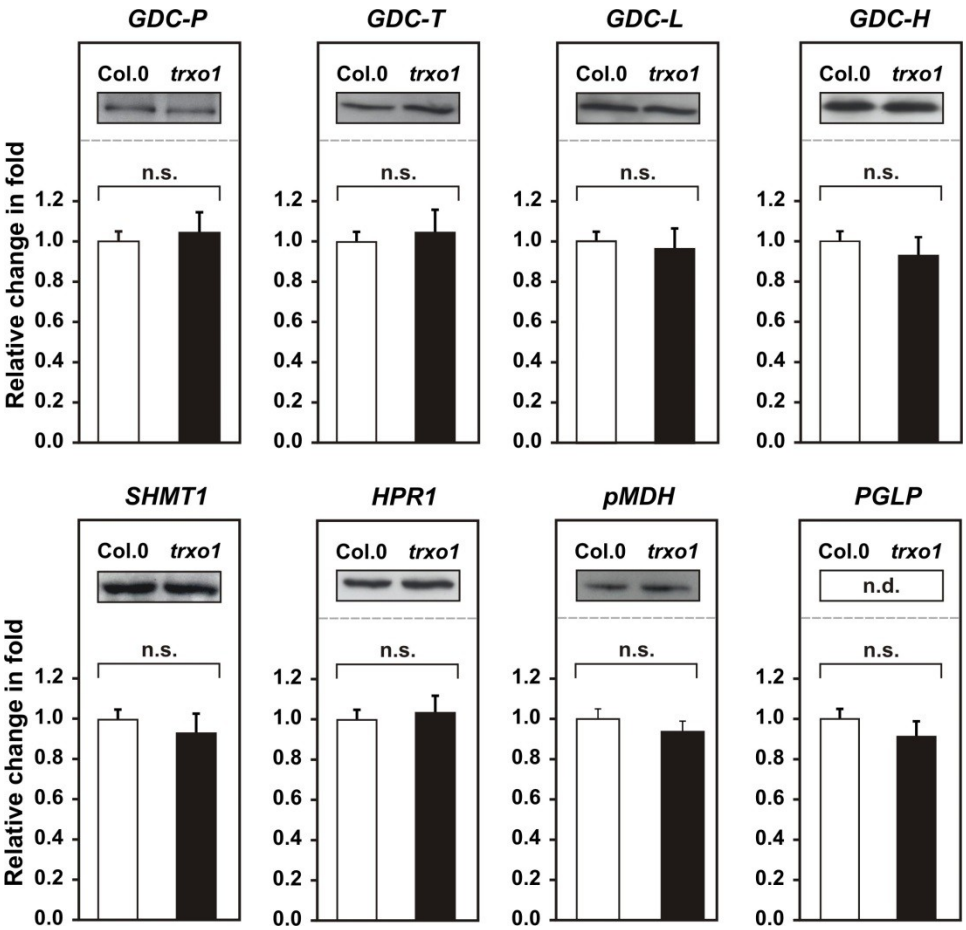


Figure 3. Expression of selected photorespiratory enzymes on the mRNA and protein level.

Plants were grown in normal air (390 ppm CO_2) with a 10/14 h day/night cycle. After 8 weeks (growth stage 5.1, Boyes et al., 2001), leaf-material was harvested at the end of the day (9 h illumination) and used for subsequent mRNA and protein extraction. Shown are mean values ± SD (n = 3) of mRNA expression determined by qRT-PCR analysis and representative immunoblots from the *trxo1* mutant compared to the control (n.s. – not significant; n.d. – not determined).

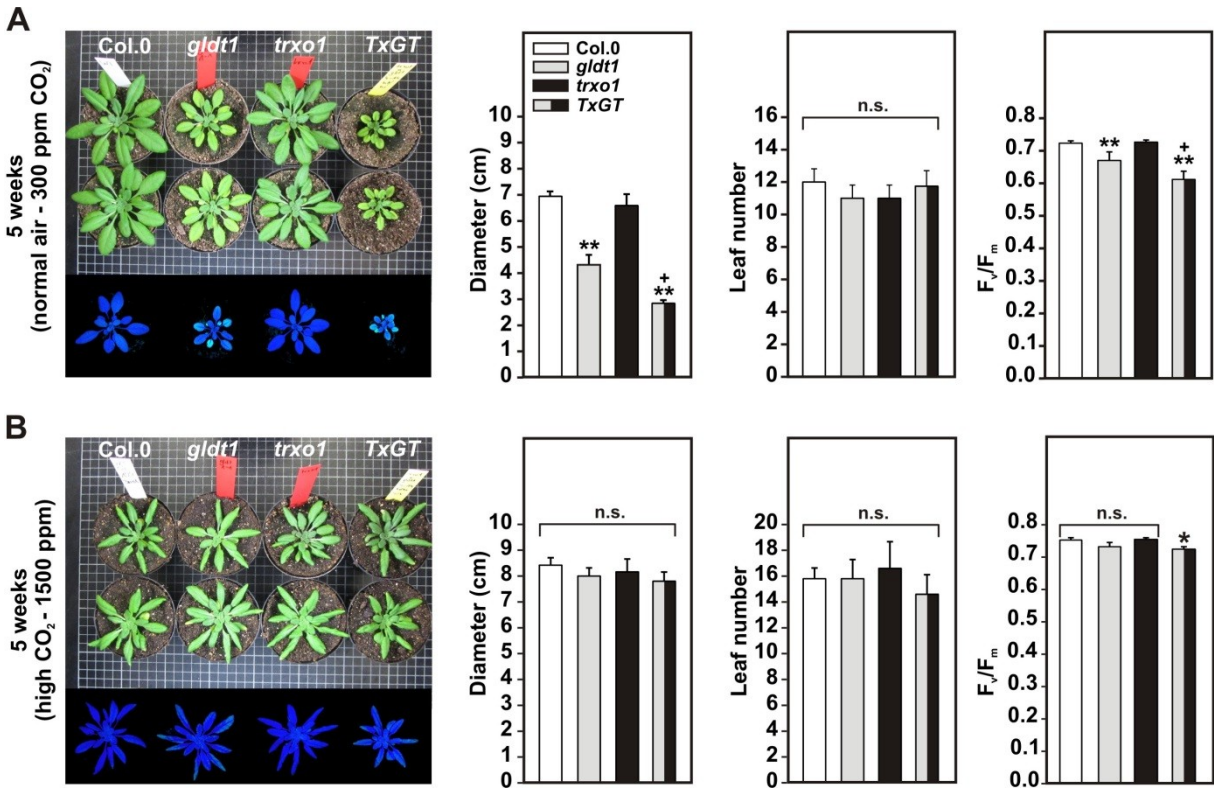


Figure 4. Phenotype, growth and chlorophyll a fluorescence of the *TxGT* double mutant.

Plants were grown in **(A)** normal air (390 ppm CO_2) or **(B)** high CO_2 (1500 ppm, HC) with a 10/14 h day/night cycle. After 5 weeks plants were photographed, rosette diameters and total leaf-numbers determined and chla fluorescence measurements carried out. Shown are mean values ± SD (n > 5). Asterisks indicate values significantly different from the control (*p < 0.05; **p < 0.01; n.s. – not significant) and plusses between the *gldt1* single and the *TxGT* double mutant ($^{+}$p < 0.05).

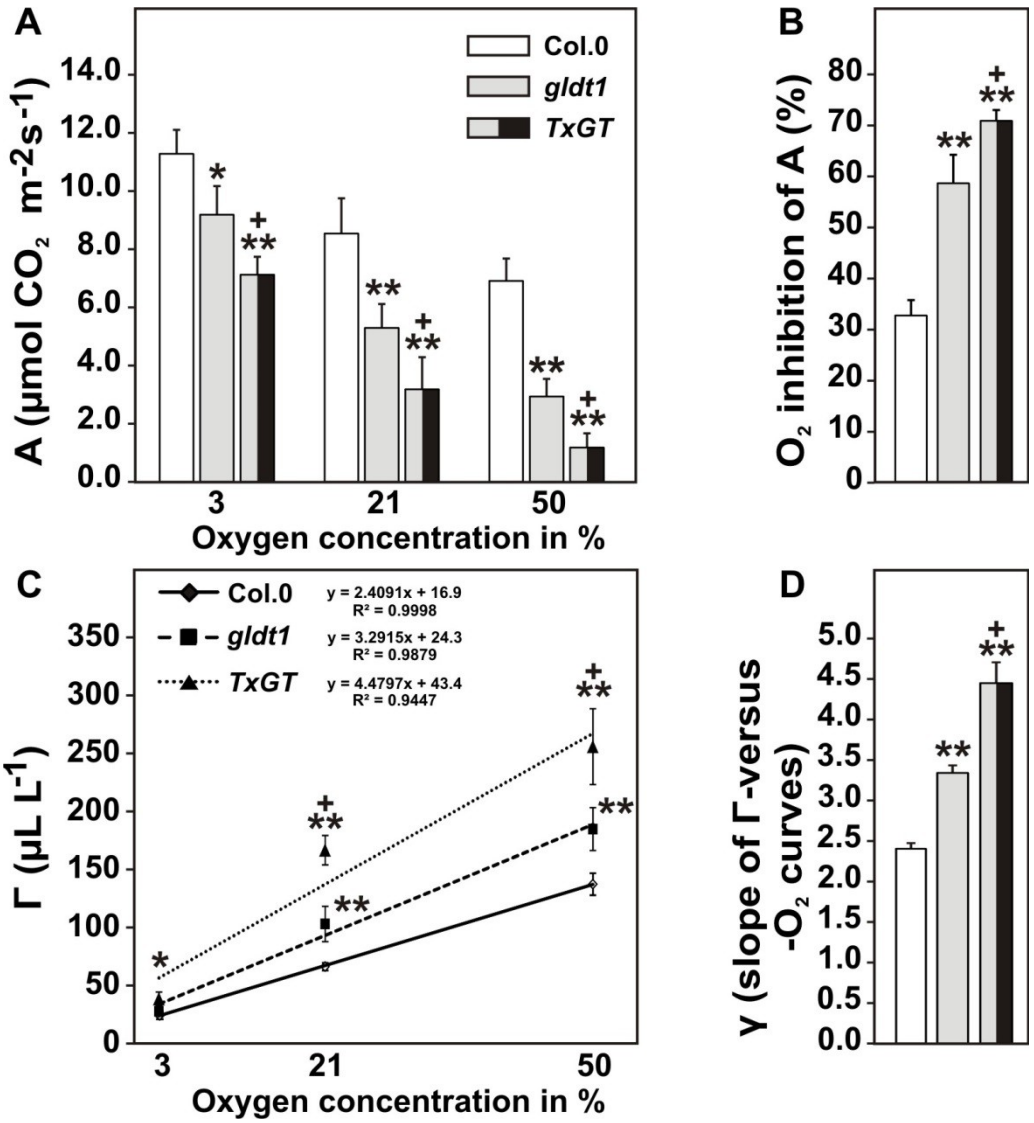


Figure 5. Oxygen-dependent gas exchange of *gldt1*, *TxGT* and the wild type.

Plants were grown in high CO_2 (1500 ppm) with a 10/14 h day/night cycle. After 7 weeks (growth stage 5.1, Boyes et al., 2001), plants were transferred to normal air (390 ppm CO_2) and used for gas exchange measurements at varying oxygen concentrations (3%, 21%, and 50%, balanced with N_2) after one week acclimation to the altered atmosphere. Mean values ± SD (n = 5-8) are shown for **(A)** net CO_2 uptake rates (A), **(B)** oxygen inhibition of A, **(C)** CO_2 compensation points (Γ) and **(D)** slopes of the Γ-versus-oxygen concentrations (γ). Asterisks indicate significant alterations of the mutants to the wild type according to Student's *t*-test (*p < 0.05, **p < 0.01) and plusses between the *gldt1* single and the *TxGT* double mutant ($^{+}$p < 0.05). For details on the calculation of oxygen inhibition and γ see material and methods section.

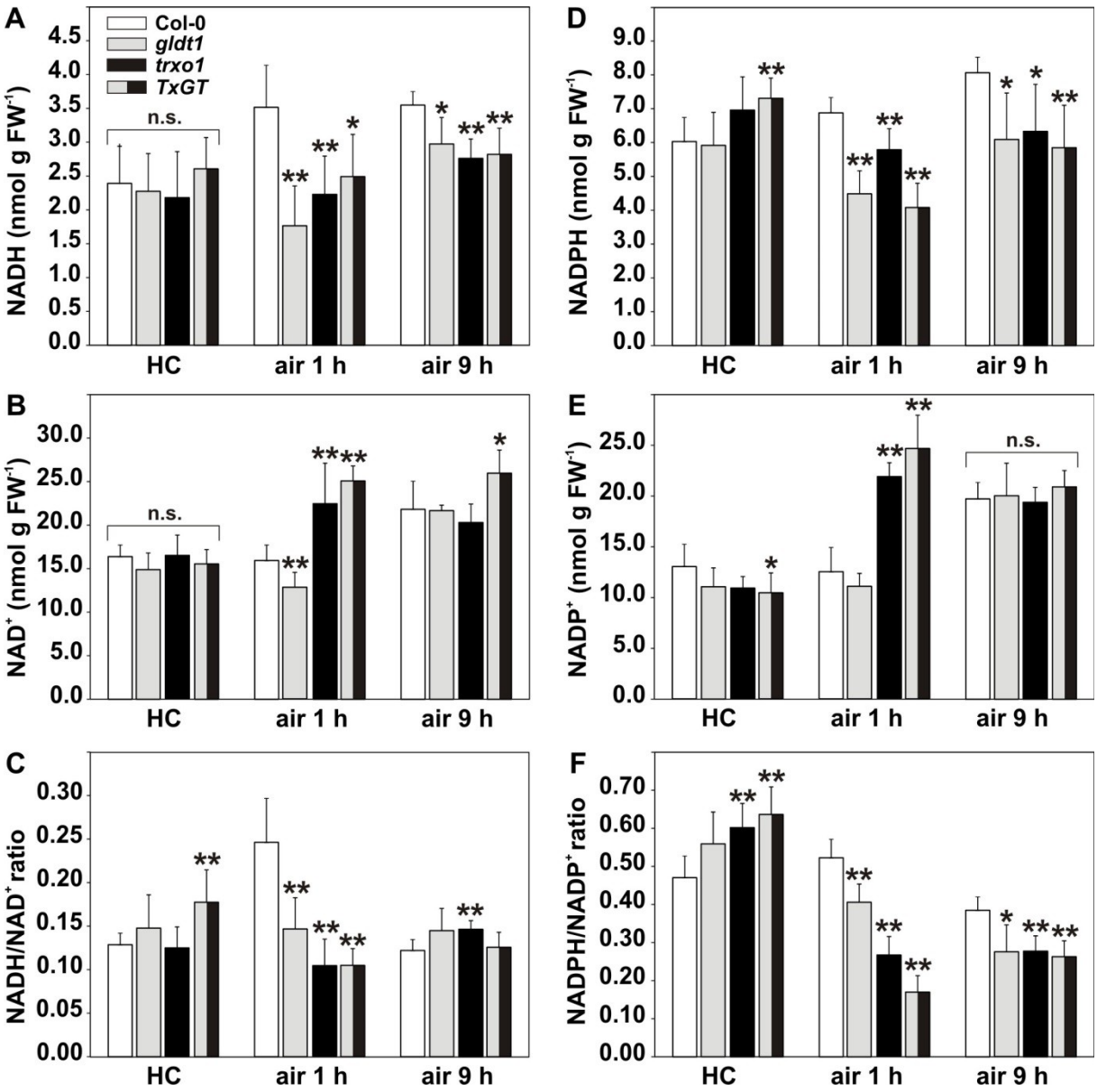


Figure 6. Pyridine nucleotide contents in wild type, *gldt1*, *trxo1* and *TxGT* plants during CO_2 transition.

Plants were grown in high CO_2 (1500 ppm, HC) with a 10/14 h day/night cycle. After 8 weeks (growth stage 5.1, Boyes et al., 2001) plants were transferred in normal air (390 ppm CO_2) with otherwise equal conditions. Leaf-material was harvested in HC (9 h light) and in normal air (1 and 9 h light), respectively. Shown are mean values ± SD (n > 6) of pyridine nucleotides (NAD^+, NADH, $NADP^+$ and NADPH) quantified by spectrophotometric analysis. Asterisks indicate significant alterations of the mutants to the wild type according to Student's *t*-test (*p < 0.05, **p < 0.01, n.s. – not significant).

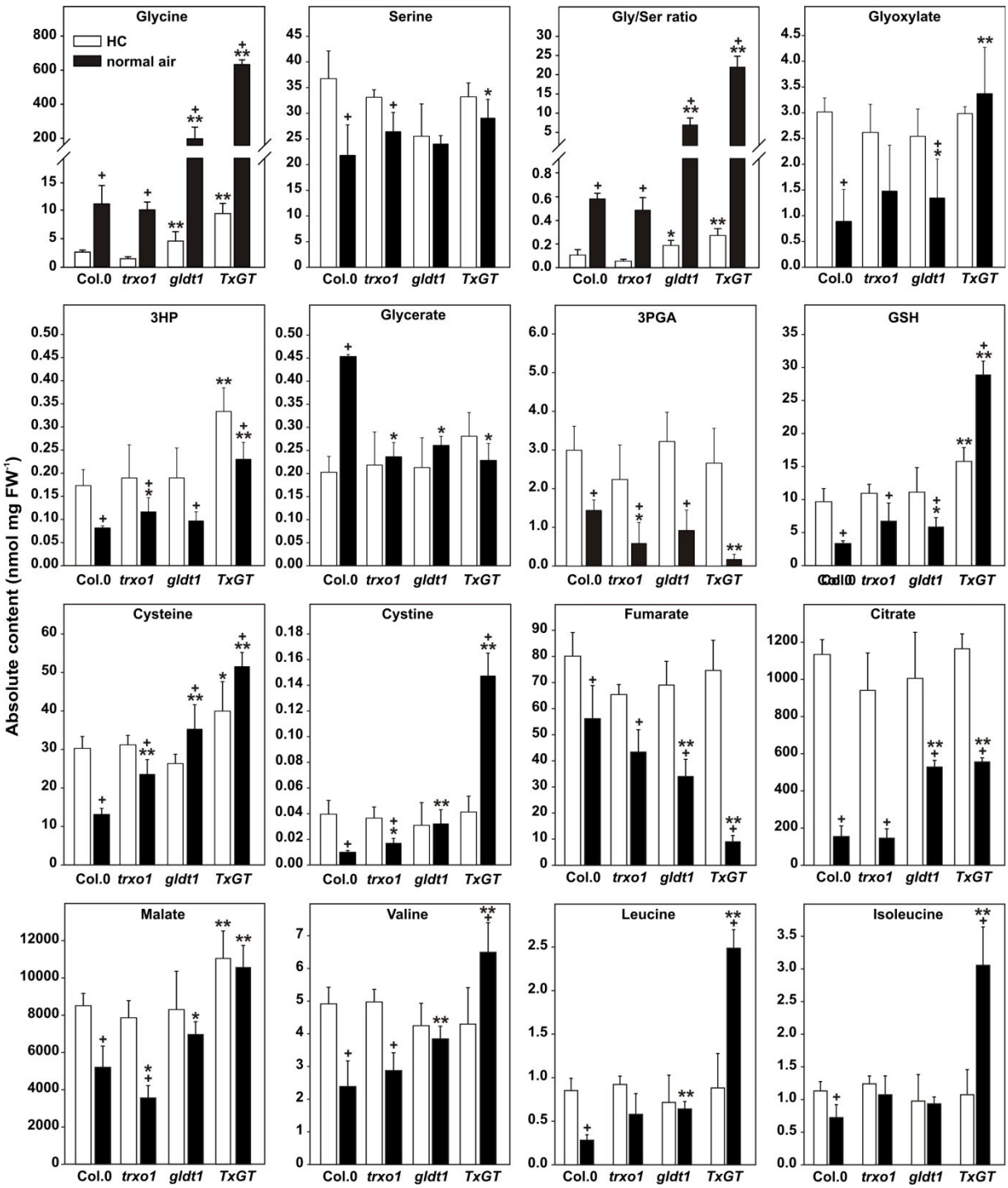


Figure 7. Levels of selected metabolites in leaves of the wild type, *trxo1*, *gldt1* and *TxGT* mutants grown in HC and normal air.

Plants were grown in high CO_2 (1500 ppm, HC) and normal air (390 ppm CO_2) with a 10/14 h day/night cycle. After 8 weeks (growth stage 5.1, Boyes et al., 2001), leaf-material was harvested in both conditions after 9 h illumination. Shown are mean values ± SD (n > 4) of selected metabolites quantified by LC-MS/MS analysis. Asterisks indicate significant alterations of the mutants to the wild type in each condition according to Student's *t*-test

(*p<0.05; **p<0.01) and plusses between HC and normal air values of each genotype (*p<0.05). For a more comprehensive dataset including statistical evaluation please compare Supp. Table 2.

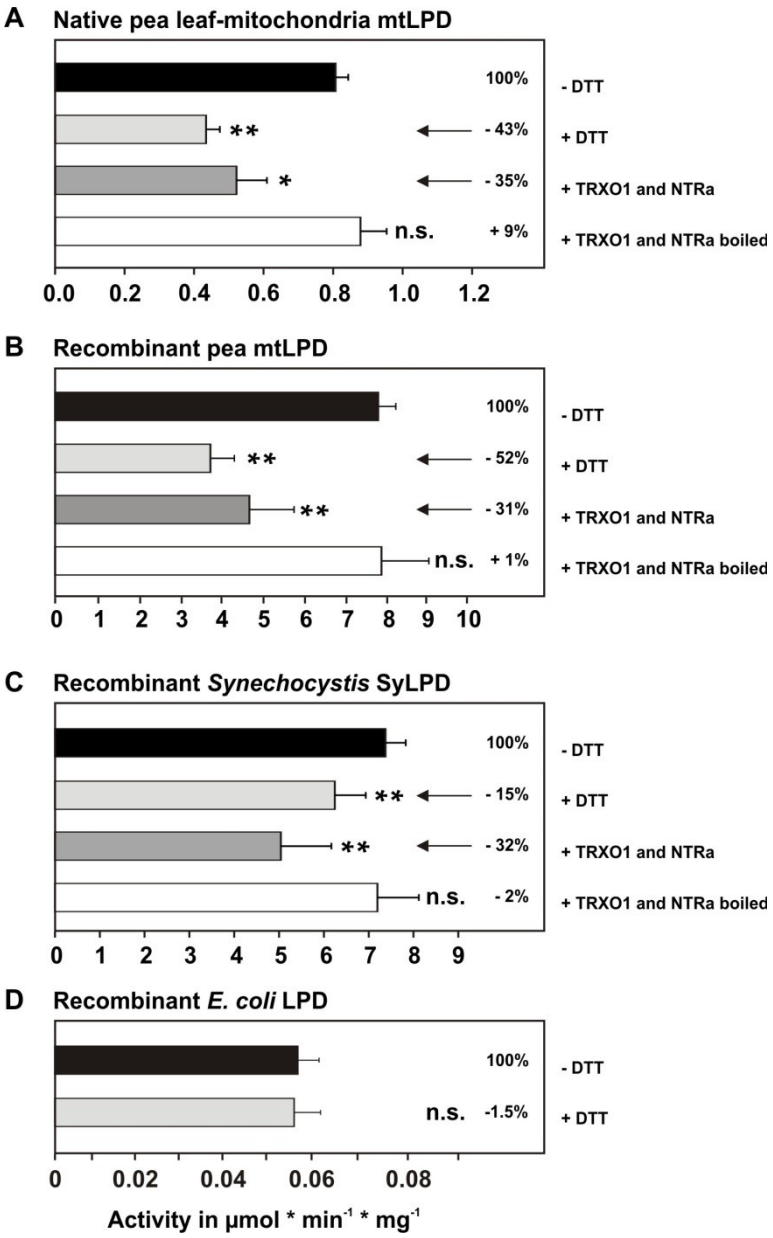


Figure 8. Redox-regulation of LPD from pea, Synechocystis and *E. coli*.

The activity of LPD proteins was determined in **(A)** pea leaf-mitochondria or of recombinant proteins produced through heterologous expression in *E.coli* and affinity purification from **(B)** pea, **(C)** Synechocystis and **(D)** *E.coli*, respectively. Shown are mean values ± SD (n > 4) of LPD activity without or after addition of DTT and recombinant native or boiled TRXo1 and NTRa. Asterisks indicate significant alterations to the control according to Student's *t*-test (* $p < 0.05$, ** $p < 0.01$, n.s. – not significant). For experimental details see material and methods section.

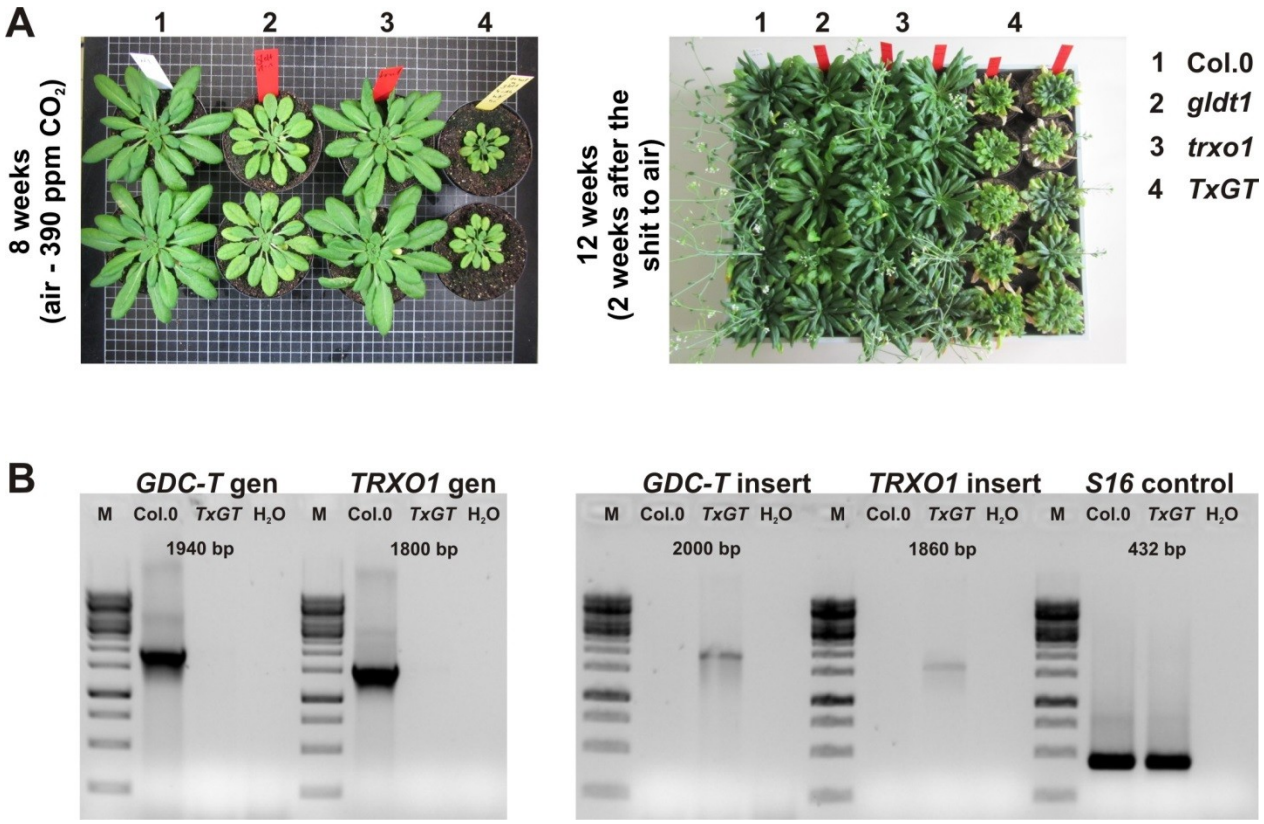
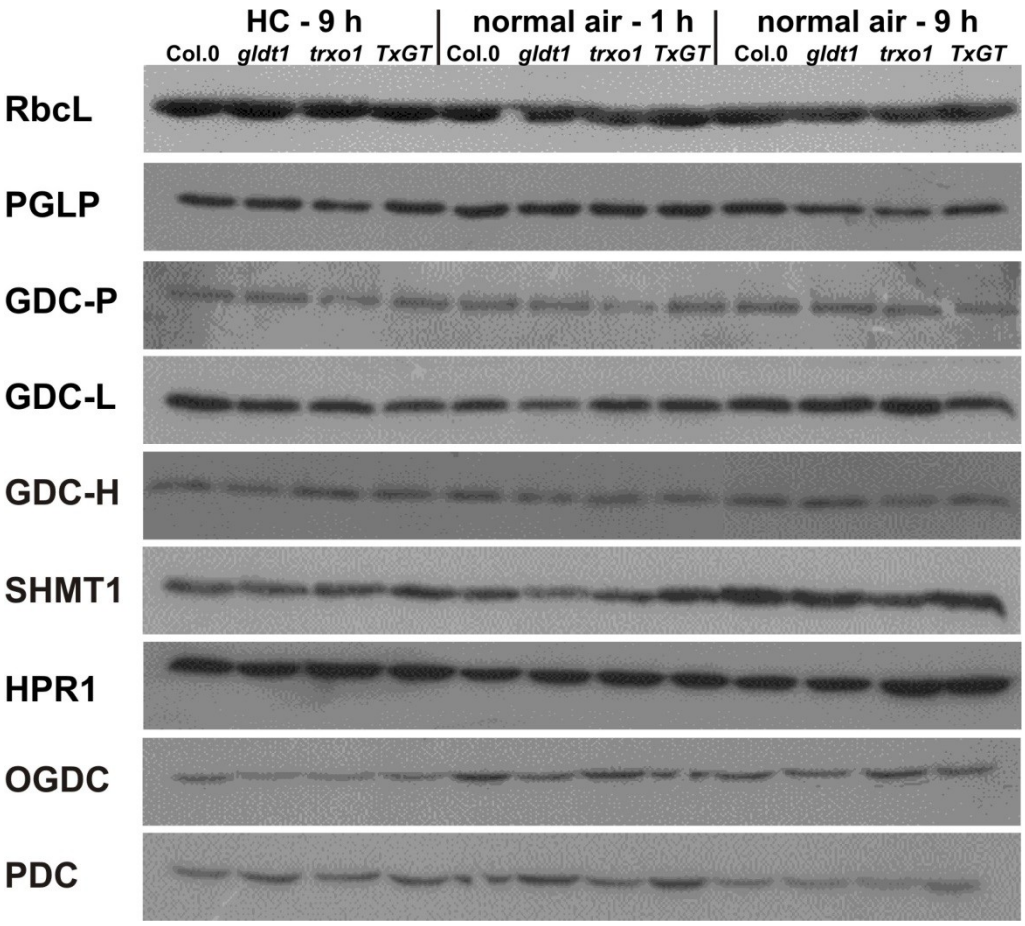


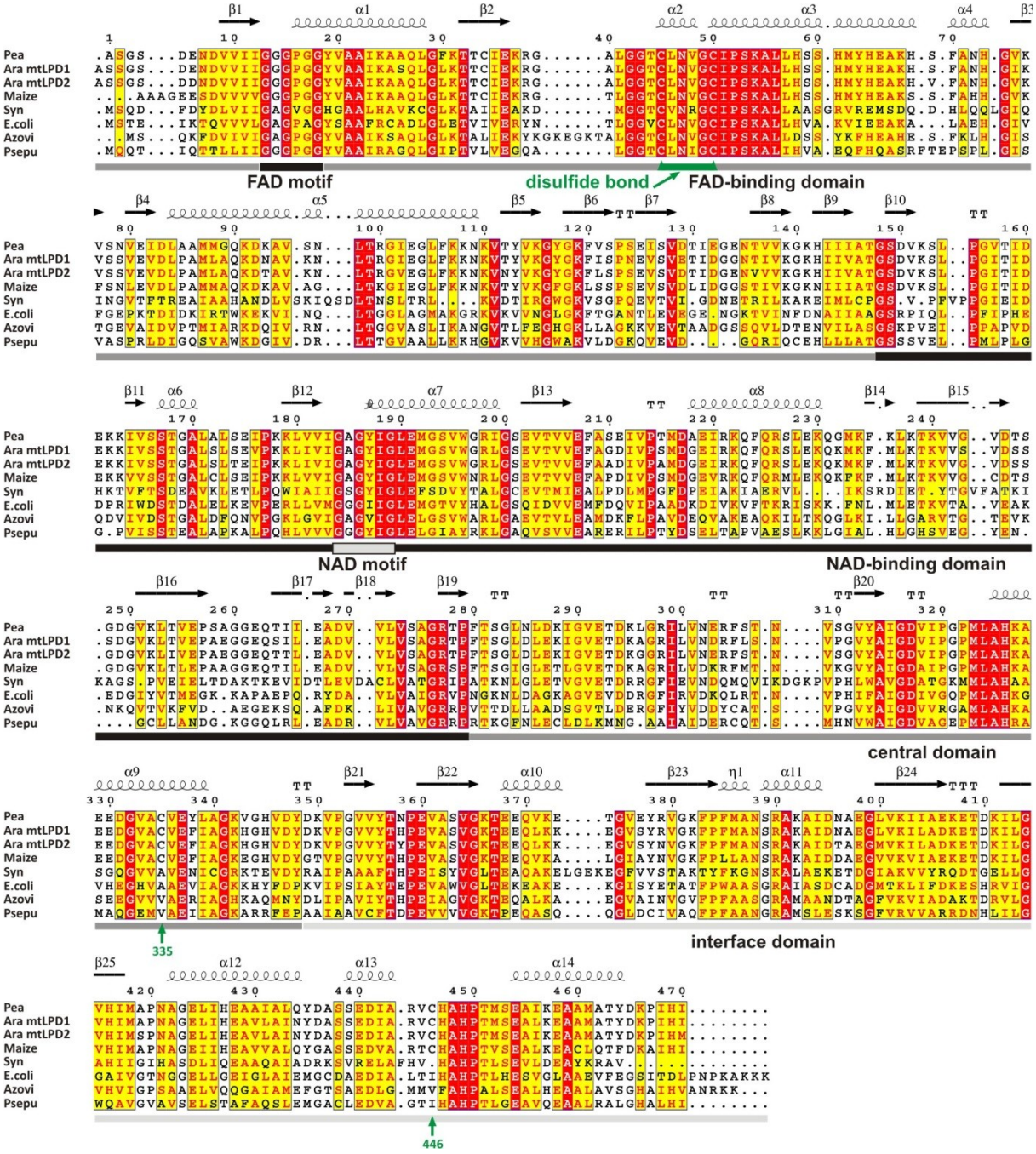
Figure 1. Phenotype and PCR verification of the *TxGT* mutant.

(A) Phenotype of the *TxGT* mutant compared to the *gldt1* and *trxo1* single mutants and the wild type after 8 weeks (left panel) in normal air (390 ppm CO_2) and after 12 weeks (right panel), 2 weeks after the transfer into normal air. **(B)** PCR verification of the *TxGT* mutant and the corresponding loading control (40S ribosomal protein *S16* gene). For primer combinations and PCR conditions please see material and methods section.



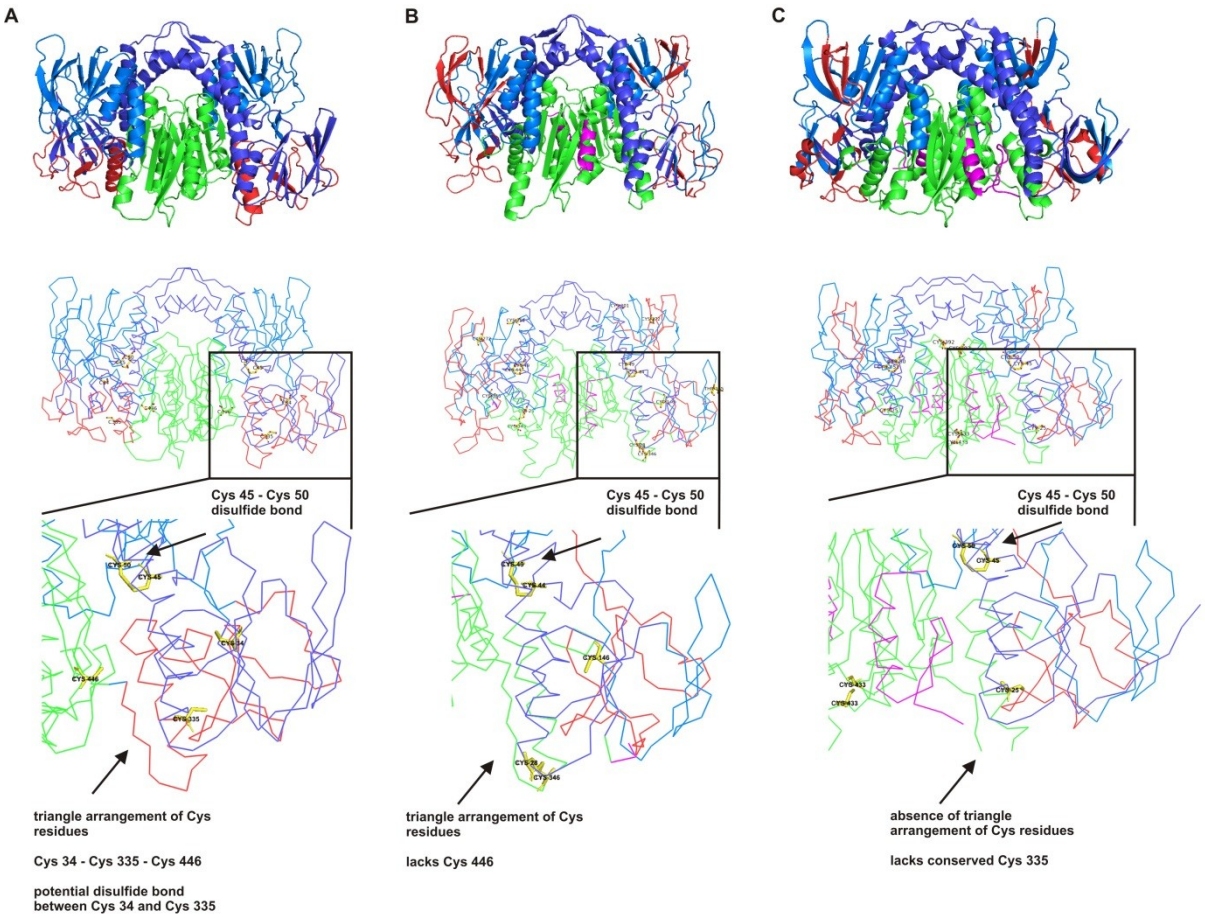
Supplemental Figure 2. Expression of selected photorespiratory and TCA cycle enzymes during CO_2 transition.

Plants were grown in high CO_2 (1500 ppm, HC) with a 10/14 h day/night cycle. After 8 weeks (growth stage 5.1, Boyes et al., 2001) plants were transferred in normal air (390 ppm CO_2) with otherwise equal conditions. Leaf-material (pools of 3 biological replicates) was harvested in HC (9 h light) and in normal air (1 and 9 h light), respectively, and used for subsequent protein extraction. Shown are mean representative immunoblots from the *gldt1*, *trxo1* and *TxGT* mutant compared to the wild type. Abbreviations: RbcL – Rubisco large subunit, PGLP – 2-phosphoglycolate phosphatase, GDC-P – glycine decarboxylase P-protein, GDC-L – glycine decarboxylase L-protein, GDC-H – glycine decarboxylase H-protein, SHMT1 – serine hydroxymethyltransferase 1, HPR1 – hydroxypyruvate reductase 1, OGDC – 2-oxoglutarate dehydrogenase complex E2 subunit, PDC – pyruvate dehydrogenase complex E2 subunit.



Supplemental Figure 3. Alignment of LPD proteins from different sources.

Protein alignment including LPD from: pea (P31023), Arabidopsis (mtLPD1 - At1g48030; mtLPD2 - AT3G17240), maize (A0A1D6MSE3), Synechocystis (P72740), *E.coli* (P0A9P0), *Azotobacter vinelandii* (C1DGW2) and *Pseudomonas putida* (Q88C17). Secondary structures were drawn using the program ESPRIT (Gouet et al., 1999).



Supplemental Figure 4. 3D structures of selected LPD proteins.

Shown are LPD 3D structure models from **(A)** pea (P31023), **(B)** Synechocystis (P72740) and **(C)** *E.coli* (P0A9P0). The structures were produced in the program SWISS-MODEL using the resolved pea protein structure as template. Further processing to resolve CYS residues was carried out using PyMOL. Arrows indicate the predicted disulfide bond between the conserved Cys 45 and Cys 50 in all organisms and the triangle arranged Cys residues (Cys 34, Cys 335 and Cys 446) present only in sequences obtained from phototrophic organisms.